Gastroenterology 2021;161:623–636

EGF and BMPs Govern Differentiation and Patterning in Human Gastric Glands

Sarah Wölffling,[1] Alice Anna Daddi,[2] Aki Imai-Matsushima,[1,3] Kristin Fritsche,[1] Christian Goosmann,[1] Jan Traulsen,[2] Richard Lisle,[2] Monika Schmid,[1] Maria del Mar Reines-Benassar,[1] Lennart Pfannkuch,[1] Volker Brinkmann,[1] Jan Bornschein,[4,5] Peter Malfertheiner,[5] Jürgen Ordemann,[6,7] Alexander Link,[5] Thomas F. Meyer,[1,8] and Francesco Boccellato[1,2]

[1]Department of Molecular Biology, Max Planck Institute for Infection Biology, Berlin, Germany, [2]Ludwig Institute for Cancer Research, Nuffield Department of Clinical Medicine, University of Oxford, United Kingdom; [3]Preemptive Medicine and Lifestyle-Related Diseases Research Center, Kyoto University Hospital, Kyoto, Japan; [4]Translational Gastroenterology Unit, John Radcliffe Hospital, Oxford University Hospitals, Oxford, United Kingdom; [5]Department of Gastroenterology, Hepatology and Infectious Diseases, Otto-von-Guericke University Hospital, Magdeburg, Germany; 6Department of Bariatric and Metabolic Surgery, Helios Klinikum, Berlin, Germany; [7]Center for Bariatric and Metabolic Surgery, Vivantes Klinikum Spandau, Berlin, Germany; and [8]Laboratory of Infection Oncology, Institute of Clinical Molecular Biology, Christian Albrechts University of Kiel and University Hospital Schleswig-Holstein, Kiel, Germany

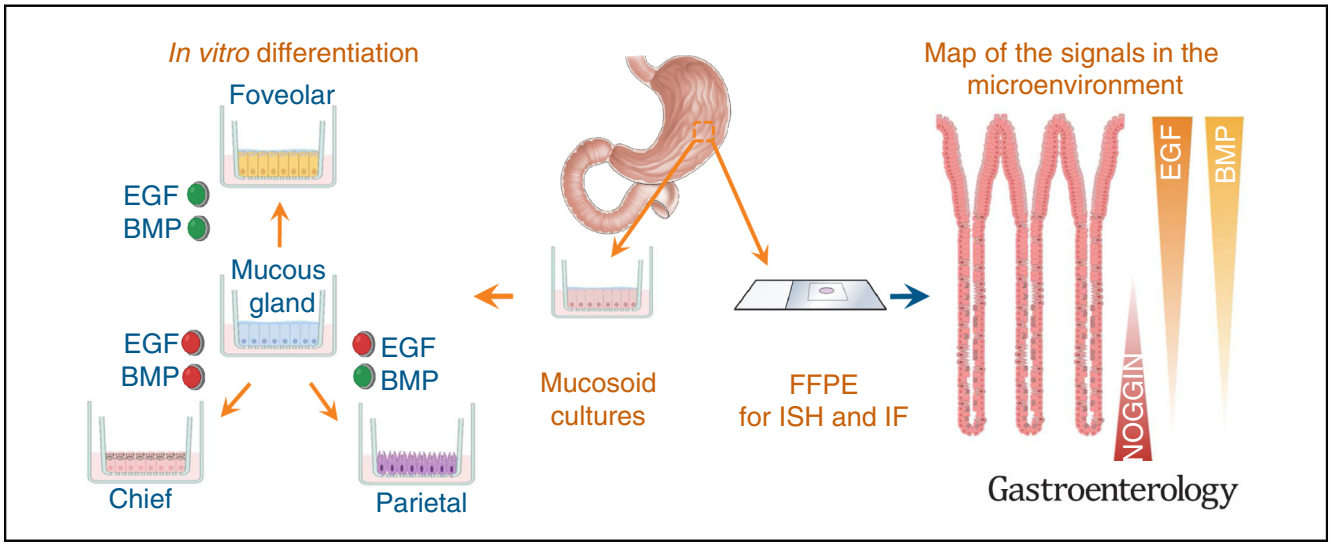

BACKGROUND & AIMS: The homeostasis of the gastrointestinal epithelium relies on cell regeneration and differentiation into distinct lineages organized inside glands and crypts. Regeneration depends on Wnt/β-catenin pathway activation, but to understand homeostasis and its dysregulation in disease, we need to identify the signaling microenvironment governing cell differentiation. By using gastric glands as a model, we have identified the signals inducing differentiation of surface mucus-, zymogen-, and gastric acid–producing cells. **METHODS:** We generated mucosoid cultures from the human stomach and exposed them to different growth factors to obtain cells with features of differentiated foveolar, chief, and parietal cells. We localized the source of the growth factors in the tissue of origin. **RESULTS:** We show that epidermal growth factor is the major fate determinant distinguishing the surface and inner part of human gastric glands. In combination with bone morphogenetic factor/Noggin signals, epidermal growth factor controls the differentiation of foveolar cells vs parietal or chief cells. We also show that epidermal growth factor is likely to underlie alteration of the gastric mucosa in the precancerous condition atrophic gastritis. **CONCLUSIONS:** Use of our recently established mucosoid cultures in combination with analysis of the tissue of origin provided a robust strategy to understand differentiation and patterning of human tissue and allowed us to draw a new, detailed map of the signaling microenvironment in the human gastric glands.

Keywords: Stomach; Epithelium; Mucosoids; Epidermal growth factor, EGF; Bone moprhogenetic protein , BMP Noggin; Differentiation; patterning Gastric Cancer.

The cellular composition and the homeostasis of epithelia depend on the activity of regenerative cells that proliferate and differentiate into different lineages. In the human stomach, the epithelium is organized into deep

Abbreviations used in this paper: **AG, atrophic gastritis; *ATP4B*, ATPase H+/K+ transporting subunit β gene; BMP, bone morphogenetic protein; CG, chronic gastritis; EGF, epidermal growth factor; EGFR, epidermal growth factor receptor; MEKi, inhibitor of MEK; mRNA, messenger RNA; PGC, pepsinogen C; TGF, transforming growth factor.**

Most current article

0016-5085
https://doi.org/10.1053/j.gastro.2021.04.062

WHAT YOU NEED TO KNOW

BACKGROUND AND CONTEXT

Previous studies using animal models have shown that stem cells in the stomach are maintained by active Wnt/β-catenin signaling pathway. Little is known about the signals promoting cell differentiation.

NEW FINDINGS

We have found that epidermal growth factor (EGF) and bone morphogenetic protein 4 (BMP4) regulate human gastric cell differentiation into the main lineages, and high EGF is likely to be the cause of loss of chief and parietal cells in atrophic gastritis.

LIMITATIONS

Genetic tracing tools can be used to identify the progenitors and the differentiation hierarchy of human gastric cells, which is not addressed in this study.

IMPACT

EGF and BMPs can also determine the shape and cell composition of other tissues. Dysregulation of these signaling molecules might dictate the changes in tissue morphology observed during infection, inflammation, and cancer.

invaginations called gastric glands populated by distinct types of cells. The part that opens to the lumen of the stomach (foveolae or "pit") comprises cells producing the moisturizing protective mucin MUC5AC.[1] Inside the gland there are chief cells secreting digestive enzymes, and another type of mucus-producing cells secreting MUC6. Proliferating cells are mostly located in the isthmus region between the gland and the foveolae. Parietal cells, which are responsible for acid production, are found in the isthmus and in the gland. The secretory functions of chief and parietal cells are regulated by hormone-producing (endocrine) cells (Supplementary Figure 1).

Cells with regenerative potential have been found at multiple sites within the gland,[2,3] and activation of the Wnt/β-catenin signaling pathway is essential for regeneration.[4–7] However, the combination of factors inducing cell differentiation into the different lineages in the gland has not yet been identified. We hypothesize that local gradients of specific differentiation factors instruct the cells to differentiate in specific locations and that these factors control the pattern of cells in the tissue. Studying differentiation and patterning of human tissues is extremely challenging due to the obvious impracticability of lineage-tracing experiments. Therefore, knowledge usually relies on the transposition of concepts from mouse models. Studying human epithelia using human-derived models is a biologic challenge, but is essential to understand human diseases to enable translational impact. Human organoids and other advanced cell cultures are addressing this challenge.[7–11] Here we use recently established mucosoid cultures,[7] which are human stem-cell–based models reminiscent of an in vivo mucosal epithelial barrier. Cells in mucosoids are contiguous and are cultivated at an air–liquid–interface to form a polarized monolayer on a porous Transwell (Millipore). The apical side is characterized by typical accumulation of epithelial mucus. When exposed to niche factors mimicking the in vivo microenvironment, cells in mucosoids are capable of multilineage differentiation and can be expanded and propagated infinitely.[7] By testing the role of differentiation factors in mucosoid cultures and analyzing the origins of those factors in the original gastric tissue, we show that epidermal growth factor (EGF), bone morphogenetic protein (BMP) and Noggin can explain the organization of cell types within gastric glands.

Materials and Methods

Treatment of Mucosoid Cultures to Induce Secretory Cell Lineage Differentiation

Primary gastric epithelial cells were grown as mucosoid cultures for a minimum of 2 weeks before treatments were started to induce differentiation. Foveolar cell differentiation was induced in antrum and corpus mucosoids by depletion of WNT3A and RSPO1 from the medium for 7 or 12 days, as described previously for organoids.[5,6] Fifty percent of the medium was changed every 3 days. For secretory cell lineage differentiation, corpus mucosoids were treated with differentiation medium for 12 days with 50% medium change every 3 days. Briefly, mucosoids were treated with different concentrations of Noggin (0–150 ng/mL) in the presence or absence of EGF. Alternatively, Noggin was depleted from the medium and 2 μM PD0325901 (inhibitor of the kinase MEK [MEKi]; Sigma) was added in the presence or absence of 50 ng/mL BMP4 (Gibco). Corpus mucosoids treated with Noggin-depleted medium and supplemented with PD0325901 (2 μM) and BMP4 (50 ng/mL) were further stimulated with histamine (1 mM; Sigma) to activate gastric acid secretion.

Results

Gene Expression in Mucosoid Cultures Reflects the Tissue of Origin

In previous work, we isolated and cultivated epithelial cells from the antrum of the stomach into mucosoids.[7] Antrum glands consist mainly of mucus producing cells, while corpus glands contain also chief and parietal cells.[12] To understand the differences between these 2 regions in the stomach, we obtained gastric sleeve resection samples from 11 obese patients (Supplementary Table 1). Two-by-two centimeter portions of the gastric mucosa from the center of the corpus and from the antrum (Figure 1*A*) were processed to cultivate mucosoids, as we have described previously[7]; both antrum and corpus epithelia were cultivated using identically composed growth medium (Supplementary Table 2). Histologic samples of the corpus can be easily distinguished from the antrum by the gland height (Figure 1*B* and *C*). Consistent with our previous findings for antrum-derived mucosoids,[7] both antrum- and corpus-derived mucosoids are populated by MUC6$^+$ cells, which is typical of glands in both stomach regions (Figure 1*D* and *E*). We compared the gene expression signatures of the antrum- and corpus-derived mucosoids by microarray and found a

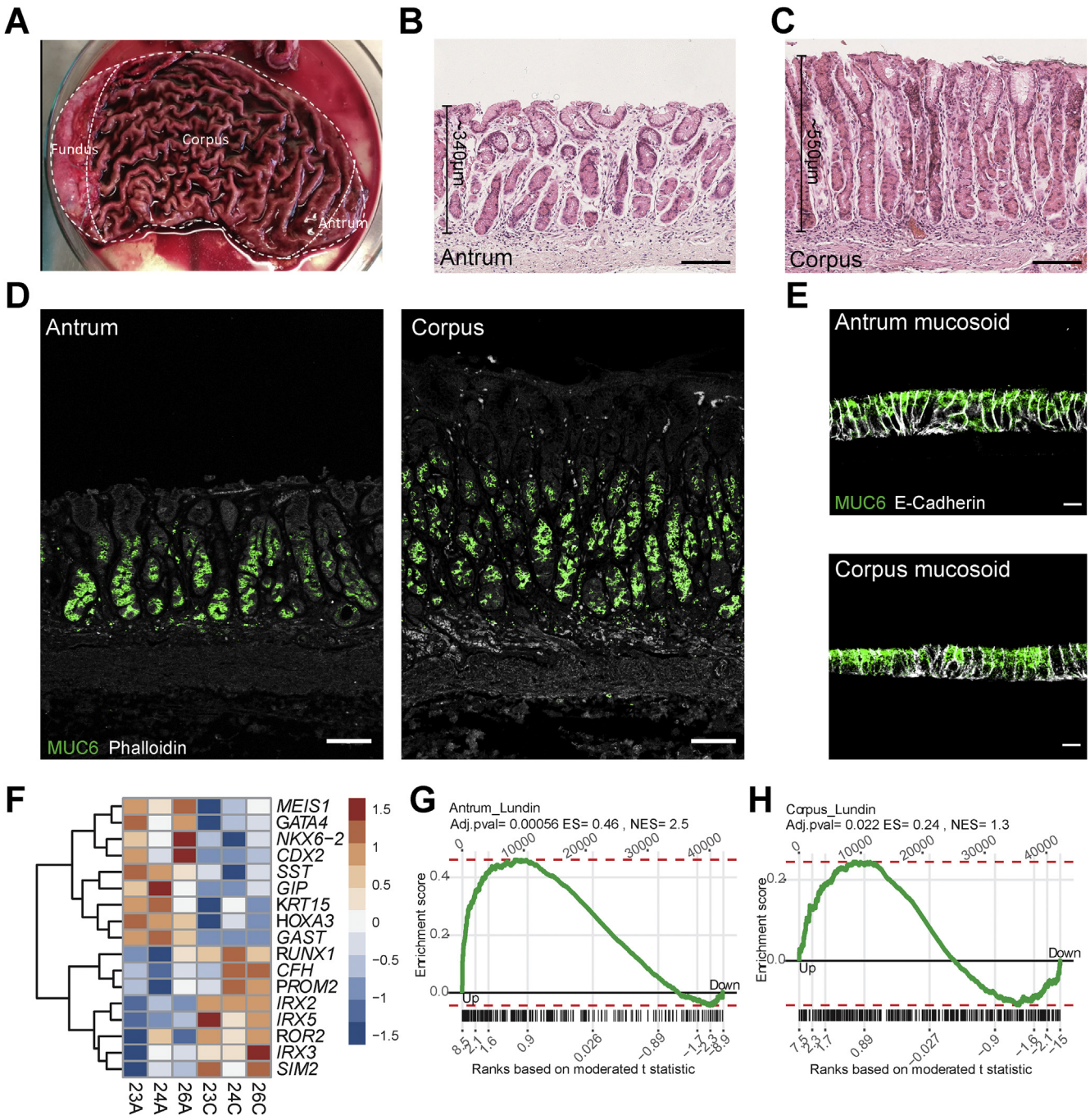

Figure 1. Corpus- and antrum-derived mucosoids maintain their identity in culture. (*A*) A human sleeve resection: mucosoids were generated from epithelial cells of the middle part of the corpus and from the antrum. (*B, C*) H&E staining showing glands of the gastric corpus and antrum. *Scale bar:* 100 μm. (*D*) Immunofluorescence analysis for MUC6 showing position of gland mucus cells in the antrum and corpus. Phalloidin shows actin filaments. (*E*) Mucosoids cultured from cells from antrum or corpus cells after 14 days, stained for MUC6 and E-cadherin. *Scale bar:* 5 μm. (*F*) *Heat map* showing the most differentially expressed genes between 3 antrum-derived and 3 corpus-derived mucosoid cultures. (*G, H*) Gene set enrichment analysis comparing antral (*G*) or corpus (*H*) mucosoid cultures with in vivo data from Nookaew et al.[15] Gene expression in both mucosoids correlates with biopsies of matching origin (antrum normalized enrichment score [NES] = 2.5, corpus NES = 1.3).

distinct subset of genes that is consistently different between antrum and corpus mucosoids across samples derived from different patients (Figure 1*F*). As in the stomach in situ, gastrin (*GAST*) and somatostatin (*SST*) are expressed more in antrum-derived compared with corpus-derived mucosoids. Notably, transcription factors involved in endodermal patterning—including *GATA4, CDX2*, and *IRX2,3,5*[13,14]—are also differentially expressed, indicating that the cells in vitro retain a memory of their proximal (corpus) or distal (antrum) origin. Focusing on genes that are differentially expressed in antrum vs corpus gastric biopsies (based on publicly available gene expression data[15]), we found a corresponding

significant and strong enrichment of these genes when comparing antrum- and corpus-derived mucosoids (normalized enrichment score = 2.5 for antrum and 1.3 for corpus (Figure 1*G* and *H*). Thus, mucosoid cultures retain key aspects of their identity and a distinct gene expression signature typical of their tissue of origin (antrum or corpus), even when exposed to identical culture conditions, suggesting that stem cells in these regions might be distinct. As the corpus mucosoids are reminiscent of their tissue of origin, we used them to investigate factors governing differentiation of specialized cell types in human oxyntic glands.

Foveolar Cell Differentiation Depends on Bone Morphogenetic Protein Signaling

The typical abundant mucin expressed by foveolar cells is MUC5AC, whereas mucus cells in the inner part of the gland express MUC6 (Figure 2*A*). Wnt signaling plays an important role in patterning the luminal–basal axis of the gut, and its activation has been associated with enhanced regenerative properties in the intestine[16] and in the stomach.[17] We recently demonstrated that foveolar differentiation in human antrum glands is inhibited by Wnt/β-catenin pathway activation.[7] We confirmed that for the corpus-derived mucosoids, removal of Wnt ligands from the culture cocktail induced a complete change from MUC6$^+$ to MUC5AC$^+$ cells (Supplementary Figure 2*A, B,* and *C*). Given known crosstalk between Wnt and BMP signaling, and the effects of BMP inhibition on murine gastric glands,[18] we investigated whether BMP signaling influences foveolar cell differentiation in human gastric glands. Noggin is a BMP inhibitor and is essential for regeneration of organoid and mucosoid cultures. When Noggin was removed, *MUC5AC* messenger RNA (mRNA) and the number of MUC5AC$^+$ cells were increased in the mucosoids, whereas expression of the β-catenin target gene *LGR5* was reduced (Figure 2*B*, *C*, and *D*). Although *MUC6* mRNA levels were reduced in the absence of NOGGIN, the number of MUC6$^+$ cells was not significantly changed (Figure 2*B* and *D*). Expression of the BMP target gene *ID1* was increased after removal of Noggin (Figure 2*E*), indicating active epithelial BMP signaling. Therefore, Noggin prevents differentiation into MUC5AC$^+$ cells in corpus-derived mucosoids.

In human gastric tissue, we found that Noggin is highly expressed in the muscularis mucosa below the glands (Figure 2F). Interestingly, Noggin protein has not been found in the stomach mucosa in mice (or the transcript was found at trace level only),[19–22] suggesting a possible human-specific mode of regulation. We assessed whether there is a source of BMP in human gastric corpus tissue by in situ hybridization and found that *BMP4* in particular is expressed more at the isthmus region (Figure 2*G* and Supplementary Figure 3*A*). Together, these results suggest that foveolar differentiation above the isthmus is triggered by BMP ligands present in that region, which is remote from the inhibitory Noggin below the glands.

Differentiation Toward Foveolar Cells Depends on Epidermal Growth Factor Signaling

Studies of gastric gland homeostasis in mice have suggested that stimulation of the EGF receptor (EGFR) signaling pathway influences the foveolar compartment,[23] and EGF has also been implicated in human fetal gastric epithelium development.[24,25] Therefore, we tested whether EGF signaling regulates foveolar cell differentiation in human corpus glands by using mucosoid cultures. EGF is part of the mucosoid cultivation cocktail and, when we removed it, the influence of Noggin on *MUC5AC* expression was strongly reduced (Figure 3*A*); that is, removal of Noggin no longer induced significant *MUC5AC* expression. This indicates that EGF is a strict requirement for foveolar cell differentiation. Indeed, we found that levels of *MUC6* and *LGR5* remain high in the absence of EGF regardless of Noggin (Figure 3*B* and *C*), indicating that the cells retain a phenotype typical of the lower part of the gland. To confirm that the effect of EGF on foveolar differentiation is exerted through the EGFR/mitogen-activated protein kinase(MAPK) signaling pathway, we cultivated mucosoids with EGF and with/without an inhibitor of the Kinase MEK (MEKi, PD0325901). The presence of MEKi reduced the level of *MUC5AC* and increased the levels of *MUC6* and *LGR5*, similar to the absence of EGF (Figure 3*D*). Consistent with the results of quantitative real-time polymerase chain reaction, blockage of the EGFR signaling pathway completely represses MUC5AC$^+$ foveolar cell differentiation (Figure 3*E*, quantification in Figure 3*F*).

As Noggin is produced distant from the foveolae (Figure 2*F*), cells are exposed to different amounts of this BMP inhibitor, depending on their position; we therefore tested the effect of increasing concentration of Noggin with/without EGF on the expression of cell lineage-specific markers. Again, we found little expression of *MUC5AC* in the absence of EGF (Supplementary Figure 4*A*), suggesting that any source of EGF in the gland must be close to the foveolar compartment. By contrast, the level of *MUC5AC* correlated inversely with the level of Noggin in the presence of EGF (Supplementary Figure 4*A*). In the same experimental setup, the levels of *MUC6* and *LGR5* decrease under conditions in which *MUC5AC* increases, consistent with the incompatibility of foveolar and inner-gland differentiation programs (Supplementary Figure 4*B* and *C*).

To relate these observations in mucosoids to the in vivo situation, we examined expression of the EGFR ligands *EGF* and transforming growth factor–α (*TGFA*) in the tissue of origin by immunofluorescence and in situ hybridization. Both ligands are more highly expressed at the foveolae and isthmus region than lower in the gland (Figure 3*G* and Supplementary Figure 3*B* and *C*, hybridization controls in Supplementary Figure 3*D* and *E*).

To test the role of EGF in mucin production by foveolar cells, we analyzed the apical mucous secretome. We treated mucosoids for 12 days with/without MEKi in the absence of Noggin and analyzed the accumulated mucus by mass spectrometry. Consistent with our results of quantitative real-time polymerase chain reaction, inhibition of the EGFR signaling pathway through MEKi abolished secretion of the typical foveolar mucin MUC5AC and other typical foveolar proteins TFF1 and GKN1 (Figure 3*H, I,* and *J*).

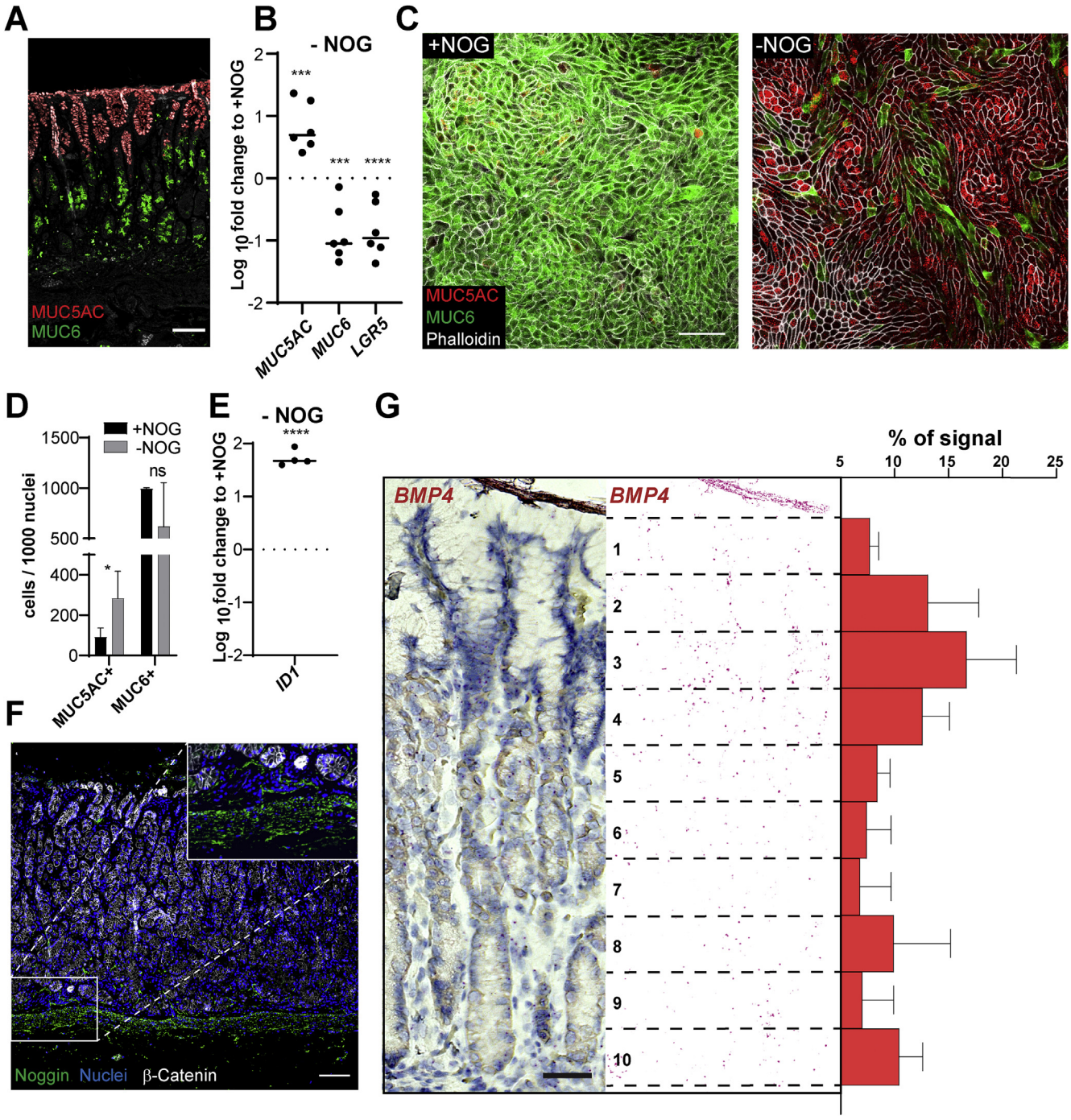

Figure 2. Noggin represses foveolar cell differentiation. (*A*) A section of a corpus gland stained for MUC5AC and MUC6. *Scale bar:* 100 μm. (*B*) Quantitative real-time polymerase chain reaction (qPCR) analysis of *MUC5AC*, *MUC6*, and *LGR5* expression after removal of Noggin (NOG) from the cultivation medium for 12 days. Results are expressed in $\log_{10}$-fold change relative to the +NOG sample. (*C*) Mucosoids cultivated in parallel with (150 ng/mL) and without Noggin for 12 days, fixed and stained whole mount for MUC5AC (*red*), MUC6 (*green*), and Phalloidin 647 (*white*), imaged from above. *Scale bar:* 25 μm. (*D*) Quantification of $MUC5AC^+$ and $MUC6^+$ cells in (*C*). Mean value $\pm$ SD of n = 4 l replicas are shown. (*E*) qPCR analysis of the BMP target gene *ID1* expression after removal of Noggin from the cultivation medium for 12 days, expressed as fold-change relative to the +NOG sample. (*F*) Immunofluorescence staining of human gastric corpus section for Noggin (*green*). Membrane and nuclei are stained with an anti–β-catenin antibody and 4′,6-diamidino-2-phenylindole, respectively. *Scale bar:* 100 μm. (*G*) *Left:* RNAscope in situ hybridization using probes detecting *BMP4* and hematoxylin staining of a human corpus gastric section *Scale bar:* 50 μm. *Center:* RNA signal deconvolution (Supplementary Material) of the *image* on the *right*. *Right:* Quantification of the signal distribution from 4 sections, divided into 10 regions of interest (ROIs) (Supplementary Material). The distribution of the signals between the ROIs is statistically different from a random distribution (1-way analysis of variance): $P = .0019$. (*B, E*) *t* test, $^{***}P < .0005$; $^{****}P < .00005$.

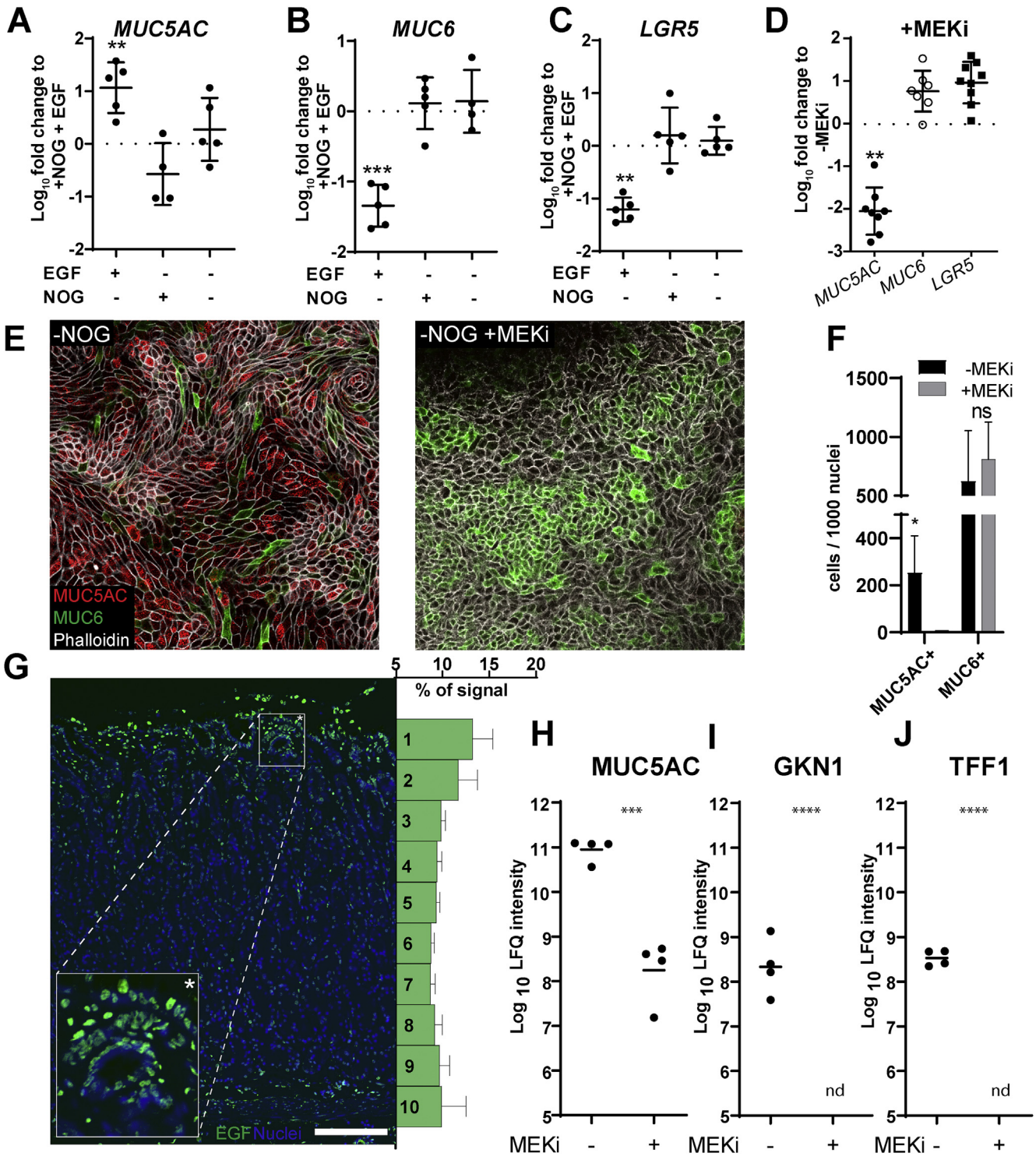

Figure 3. EGF enhances foveolar cell differentiation. (*A, B, C*) Quantitative real-time polymerase chain reaction (qPCR) analysis of *MUC5AC*, *MUC6*, and *LGR5* expression after removal of EGF and/or Noggin from the cultivation medium for 12 days. Results are expressed as $\log_{10}$ fold-change relative to the +NOG (150 ng/mL) + EGF (20 ng/mL) sample. (*D*) qPCR analysis of *MUC5AC*, *MUC6*, and *LGR5* after applying MEKi (2 μM) for 12 days. Results are expressed as $\log_{10}$ fold-change relative to the +NOG +EGF sample. (*E*) Mucosoids were cultivated in parallel without Noggin and with or without MEKi (2 μM) for 12 days. Samples were fixed and stained whole mount for MUC5AC (*red*), MUC6 (*green*), and visualized from top. Phalloidin 647 was used to visualize the cell borders. *Scale bar:* 25 μM. (*F*) Quantification of MUC5AC+ and MUC6+ cells in (*E*). Mean value ± SD of 4 biologic replicas are shown (*G*). *Left:* a section of stomach corpus, stained for EGF (*green*), shows enhanced expression of this ligand at the foveolae. Nuclei were stained with Hoechst. *Scale bar:* 100 μM. *Right:* Quantification of the signal distribution from 4 sections, divided in 10 regions of interest (Supplementary Material). Probability of a random distribution is $P = .0001$ (analysis of variance). (*H, I, J*) Mass spectrometry and label free quantification analysis of MUC5AC, TFF1, and GKN1 protein in the apical secretome of mucosoids treated with MEKi (2 μM) for 12 days compared to untreated samples. (*A, B, C, D, F, H, I, J*) *t* test, *$P < .05$; **$P < .01$; ***$P < .001$; ****$P < .0001$.

Our results suggest that high expression of EGFR ligands promotes differentiation of mucus-producing foveolar cells at the pits, which is consistent with early histopathologic reports that found EGF mostly in the luminal part of the stomach.[26]

Differentiation Toward Chief Cells by Deprivation of Epidermal Growth Factor

Chief cells are the main cell type responsible for the production of digestive enzymes (zymogens) in the stomach, as they secrete pepsin, chymosin, and lipase. They occupy half of the gland height from the base to the proliferation zone (Figure 4*A*) and they can be identified in situ by antibody staining against pepsinogen C (PGC). As we have discovered that EGF and TGFα are enriched at the pit/isthmus region, and as chief cells are positioned closer to the Noggin source in the stromal cell layer below the glands, we tested the effect of deprivation of EGF and/or Noggin on the generation of PGC$^+$ cells in corpus mucosoids. Removal of EGF enabled the expression of *PGC*, and simultaneous deprivation of Noggin had no significant effect (Figure 4*B*).

To test whether the EGFR pathway must be inactive to allow differentiation toward chief cells, we analyzed expression of PGC by immunofluorescence after treatment with an MEKi. We found that PGC expression is induced in the presence of MEKi (Figure 4*C*) and that the total number of PGC$^+$ cells increases significantly (Figure 4*D*).

We further characterized PGC$^+$ cells in the corpus mucosoids to prove that they share similarities with chief cells in function and ultrastructure. We analyzed the apical secretome of mucosoid PGC$^+$ cells obtained by inhibiting EGFR and found decreased accumulated volume of mucus (Figure 4*E*), in line with the reduced presence of MUC5AC we observed previously (Figure 3*H*). Mass spectrometry analysis of the apical secretome suggested some accumulation of the PGC protein (not statistically significant, Figure 4*F*), suggesting that PGC might not be secreted constitutively. Electron microscopy sections of the mucosoid monolayers showed dark granules on the apical side, reminiscent of zymogenic granules in vivo and different from apical mucus-transporting vesicles (Figure 4*G*).[27] Immunogold staining showed PGC specifically in the dark granules, confirming their zymogenic features (Figure 4*H*). As these cells start acquiring zymogenic granules containing pepsin precursors, we conclude that deprivation of EGF allows differentiation of cells with features of chief cells.

Bone Morphogenetic Protein Induces Differentiation Toward Parietal Cell in the Absence of Epidermal Growth Factor

Parietal cells are responsible for acid production in the stomach and they are scattered in the oxyntic glands. Specifically, they are absent from the foveolae and less abundant at the base of the gland, as observed by expression of ATPase H+/K+ transporting subunit β (HK-ATPase-β (Figure 5*A*). After removing EGF from the mucosoid cultivation cocktail, we observed a low induction of *ATP4B* expression by quantitative real-time polymerase chain reaction (Figure 5*B*), but blocking the EGFR signaling pathway by providing MEKi did not result in an increase in HK-ATPase-β^+ cells (Figure 5*C*), suggesting that a further level of regulation is needed for the correct expression of this subunit of this pump. Also, the addition of BMP4 as well as MEKi did not increase *ATP4B* mRNA (Figure 5*D*), but we found a dramatic increase in the number of HK-ATPase-β^+ cells, which suggests a post-transcriptional role of BMP4 in the regulation of the proton pump (Figure 5*E*, quantification in 5*F*). Expression of the other subunit of the pump, HK-ATPase-α, increases accordingly (Supplementary Figure 5*A*). In addition, the plasma membrane/actin cytoskeleton regulatory protein Ezrin accumulated on the apical surface, as is typically observed in resting parietal cells[28] (Supplementary Figure 5*B*).

To assess whether HK-ATPase-β^+ differentiated cells in the mucosoids form a secretory network (canaliculi) similar to parietal cells in the stomach, we analyzed the ultrastructure of cells in thin sections of mucosoids induced to express the proton pump by inhibiting the EGF signaling pathway (with MEKi) and by increasing the BMP4 concentration. We also gave a stimulus with histamine for 30 minutes before fixation to induce acid secretion. We found canaliculi surrounded by mitochondria on the apical side of the cell (Figure 5*G*). Immunogold labeling showed HK-ATPase-β in the correct location on these canaliculi (Figure 5*H*). Finally, we tested whether the HK-ATPase-β^+ cells obtained in the mucosoids were able to produce acid. After promoting differentiation, we included a pH indicator (acridine orange) and observed acid release after treating the cells with histamine (Figure 5*I*, Supplementary Figure 5*C*). Thus, the HK-ATPase-β^+, acid-producing cells obtained in vitro are analogous to parietal cells in situ. We conclude that EGF is unfavorable for differentiation toward both chief cells and parietal cells and that BMP4 activates the parietal cell differentiation program.

We further investigated whether activation of the BMP signaling pathway is the discriminant between chief and parietal lineage differentiation. We probed the expression of *BHLHA15* (also known as *MIST1*), a nuclear transcription factor expressed in chief cells, but completely excluded from parietal cells,[29] and found that the mRNA level, as well as the number of MIST1$^+$ cells, is reduced on treatment with BMP4 (Supplementary Figure 6*A* and *B*).

Epidermal Growth Factor Expression Is Increased in Atrophic Gastritis

Atrophic gastritis (AG) is a chronic inflammatory condition that is an intermediate in progression toward dysplasia and cancer caused by *Helicobacter pylori* infection. The atrophic mucosa is characterized by a marked reduction in gland height and the absence of cells involved in digestive functions, namely parietal and chief cells. The signals provoking these radical changes in tissue morphology and cell composition are unknown. As we have identified EGF and

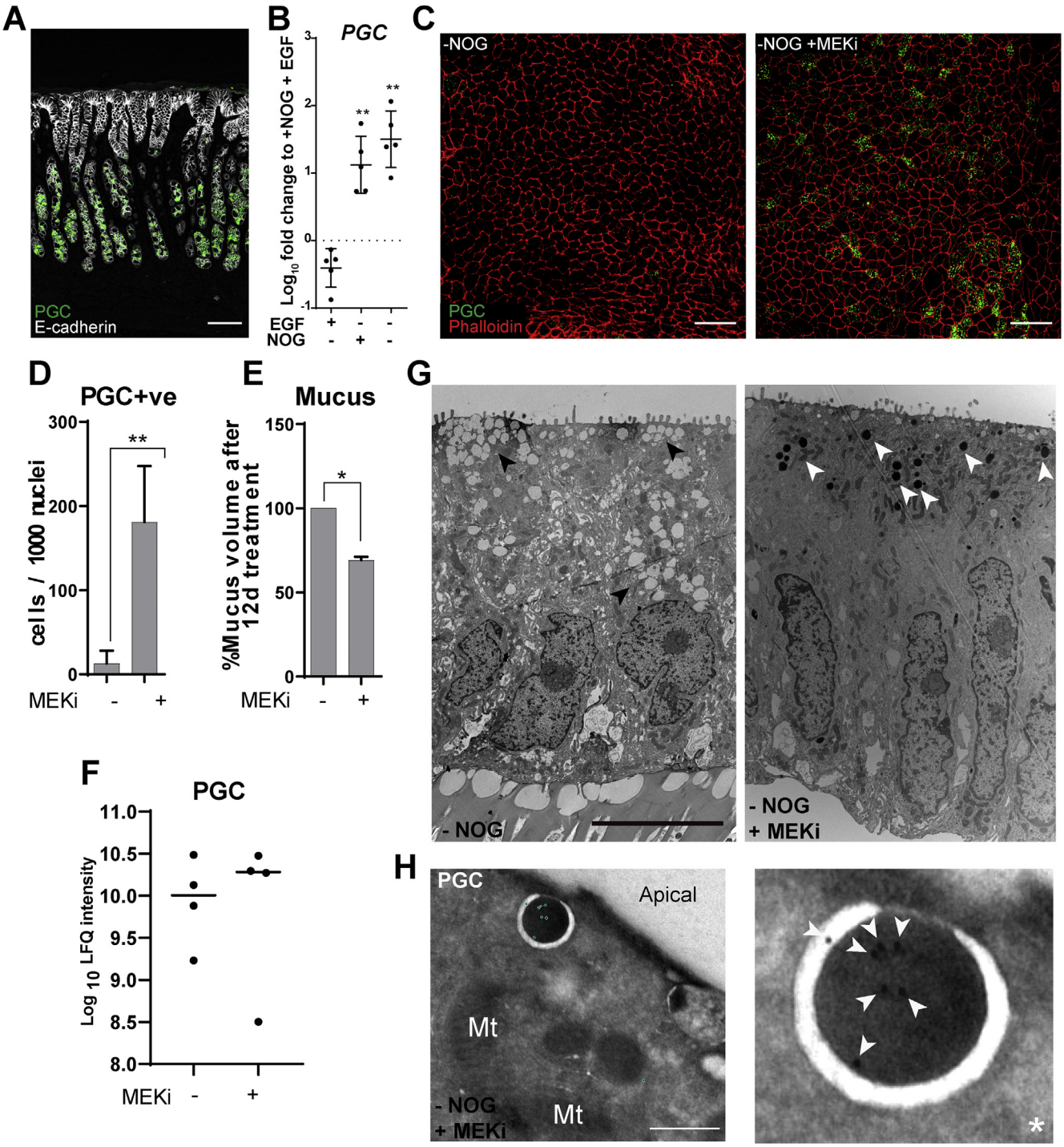

Figure 4. EGF suppresses chief cell differentiation. (*A*) Section of corpus mucosa stained for the chief cell marker PGC (*green*) and E-cadherin. *Scale bars:* 100 μm. (*B*) Quantitative real-time polymerase chain reaction analysis of *PGC* expression after removal of EGF and/or NOG from the cultivation medium for 12 days. Results are expressed as $\log_{10}$ fold-change relative to the +NOG +EGF sample. (*C*) Mucosoids cultured –NOG +EGF, with or without MEKi (2 μM) treatment for 12 days were fixed and stained whole mount and visualized from top. Phalloidin 546 was used to visualize the cells, chief cells are stained with an anti-PGC antibody (*green*). *Scale bar:* 25 μm. (*D*) Quantification (mean ± SD n = 5 biologic replicates) of the PGC^+ cells in (*C*). (*E*) Relative volume of mucus (mean ± SD n = 4) secreted by mucosoids (–NOG +EGF) after treatment with or without an MEKi for 12 days. (*F*) Mass spectrometry and label free quantification of PGC protein in the mucosoid apical secretome, with or without MEKi treatment. (*G*) Transmission electron microscopy of mucosoid samples cultured –NOG or –NOG +MEKi. Mucous vesicles (*black arrowheads, left panel*) are numerous in the absence of MEKi, whereas there are dark zymogenic granules on the apical side (*white arrowheads, right panel*) in the presence of MEKi. *Scale bar:* 2 μm. (*H*) Ultrathin (<100 nm) sections were Immunogold-labeled to detect PGC (*encircled; upper panel*). The enlargement (*lower panel*) shows PGC present in the zymogenic granules (*arrowheads*). *Scale bar:* 500 nm. Mt, mitochondria. (*B, D, E*) *t* test, $^*P < .05$; $^{**}P < .01$.

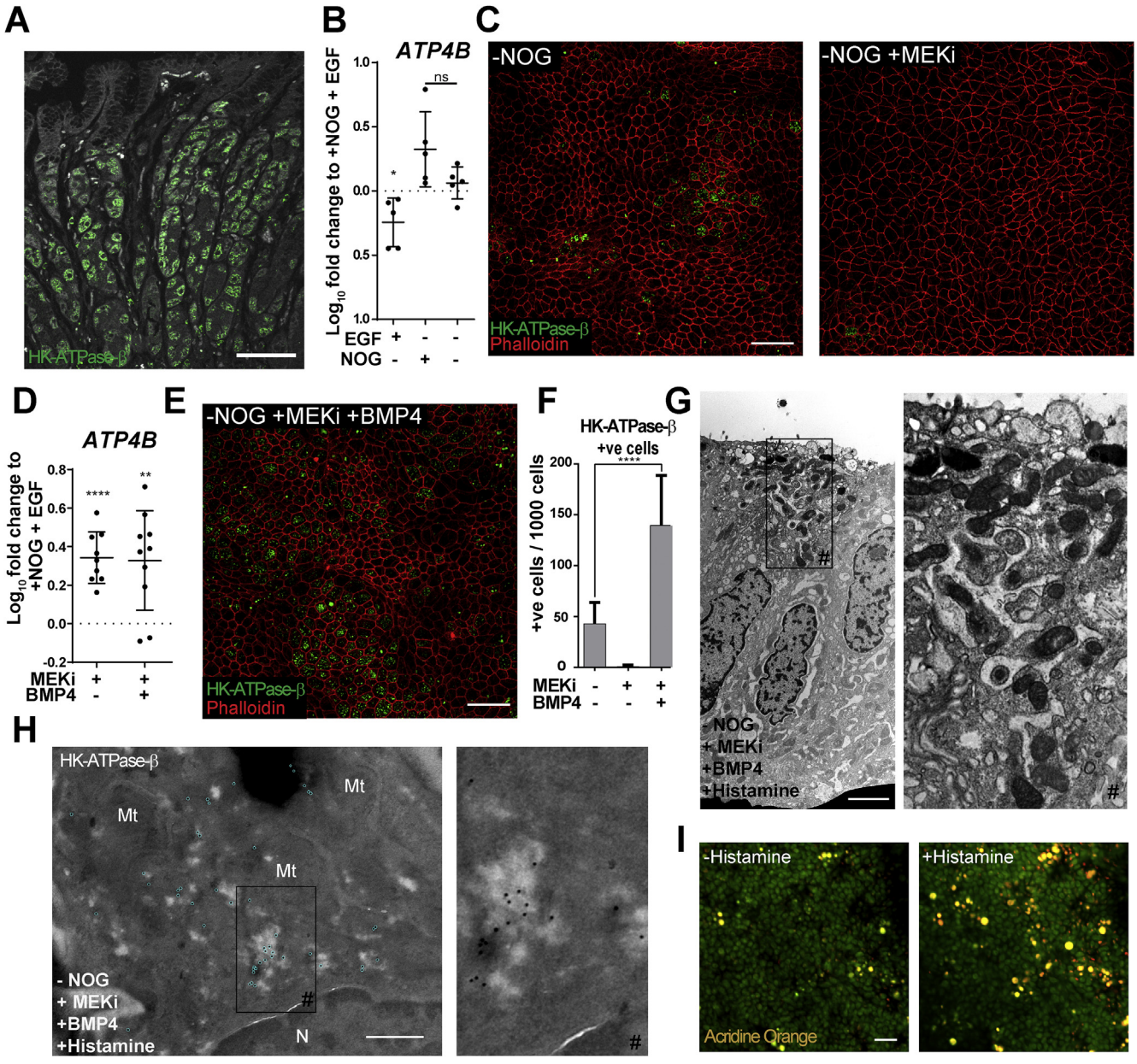

Figure 5. BMP4 enhances parietal cell differentiation in the absence of EGF signaling. (*A*) A section of oxyntic mucosa stained for the parietal cell marker HK-ATPase-β (*green*). *Scale bar:* 100 μm. (*B*) Quantitative real-time polymerase chain reaction (qPCR) analysis of *ATP4B* expression after removal of EGF and/or Noggin from the cultivation medium for 12 days. Results are expressed as $\log_{10}$ fold-change relative to the +NOG +EGF sample. (*C*) Mucosoids –NOG +EGF were treated for 12 days with or without MEKi (2 μM), fixed and stained whole mount and visualized from top. Phalloidin 546 was used to visualize the cells; parietal cells are stained with an anti–HK-ATPase-β antibody (*green*). *Scale bar:* 25 μm. (*D*) Mucosoids (–NOG +EGF) were treated with an MEKi with or without BMP4 for 12 days. Shown is qPCR for *ATP4B*, expressed as $\log_{10}$ fold-change relative to +NOG +EGF control samples. (*E*) Mucosoids cultured –NOG +EGF were treated for 12 days with MEKi and BMP4 (50 ng/mL), fixed and stained whole mount and visualized from top. Phalloidin 546 was used to visualize the cells; parietal cells are stained with an anti–HK-ATPase-β antibody (*green*). *Scale bar:* 25 μm. (*F*) Quantification (mean $\pm$ SD n = 5 biologic replicates) of HK-ATPase-β+ cells in (*C*) and (*E*). (*G*) Transmission electron microscopy of mucosoids cultured –NOG +MEKi +BMP4, plus 30 minutes 1-mM histamine stimulation, showing canaliculi (*light gray area*) and adjacent mitochondria (*dark gray*). *Scale bar:* 5 μm. (*H*) Ultrathin (<100 nm) sections were Immunogold-labeled to detect HK-ATPase-β (*encircled, left*). Enlargement (*right*) shows HK-ATPase-β present at the canaliculi (*light gray area*). Mt, mitochondria; N, nucleus. *Scale bar:* 500 nm. (*I*) Corpus mucosoid cultures cultivated with 50 ng/mL of BMP4, incubated with 1 μM of acridine orange for 15 minutes 37°C/5% CO_2, with or without activation with 10 μL 5-mM histamine solution. Fluorescence of acridine orange was excited at 488 nm and images were collected in a time series (every 10 seconds) at 500–550 nm and 600–650 nm. *Scale bar:* 25 μm. (*B, D, F*) *t* test, *$P < .05$; **$P < .05$; ****$P < .0005$.

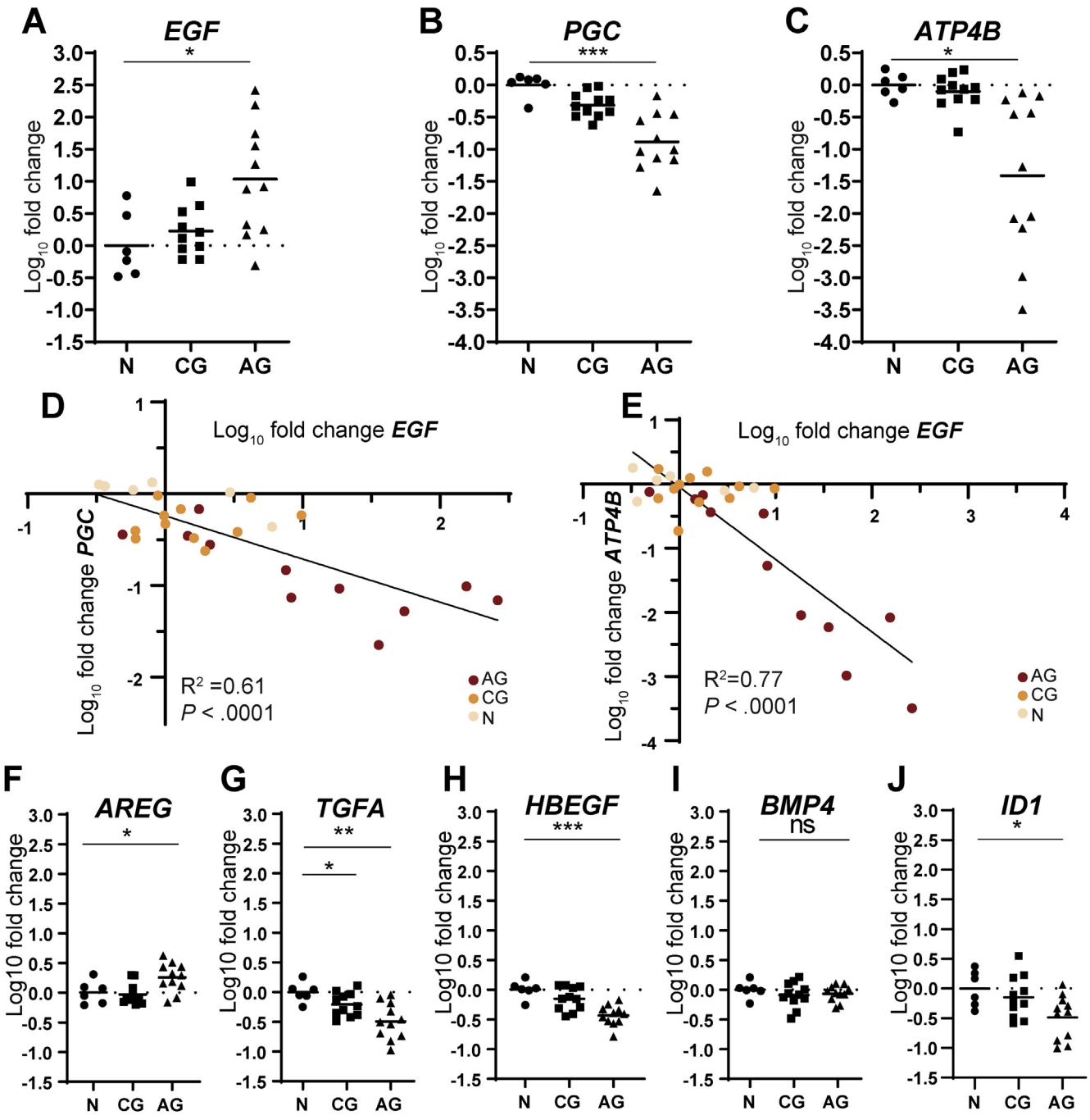

Figure 6. EGF is highly expressed in AG biopsies. Biopsies from patients diagnosed with AG (n = 11), CG (n = 8), or normal (N) gastric mucosa controls (n = 6) were processed for RNA extraction and complementary DNA synthesis. (*A, B, C, F, G, H, I, J*) *EGF*, *PGC, ATP4B, AREG, TGFA, HBEGF*, *BMP4,* and *ID1* were analyzed by quantitative real-time polymerase chain reaction and results are shown as $\log_{10}$ fold-change relative to the median of the expression of the healthy control. The median of each sample group is shown. *t* test, **P* < .05; ***P* < .005; ****P* < .0005. (*D, E*) Correlation of $\log_{10}$ fold-change of *PGC* and *EGF* (*G*) or *ATP4B* and *EGF* (*H*) for individual biopsies. To infer a linear correlation between the expressions of these markers, we calculated the R^2 coefficient of correlation and the probability *P* of deviation from 0.

BMP4/Noggin as the major epithelial signals that control foveolar vs parietal and chief cell differentiation, we compared the expression of EGFR and BMPR ligands of previously collected AG and chronic gastritis (CG) and normal biopsies.[30] Patient information and histopathologic staging according to Operative Link on Gastritis Assessment and Operative Link on Gastric Intestinal Metaplasia Assessment systems are provided in Supplementary Table 3. Interestingly, we found a remarkable overexpression of *EGF* in AG, which in some biopsies was 10–100 times higher than in normal samples (Figure 6*A*). Although CG is characterized by hypertrophy of the gastric

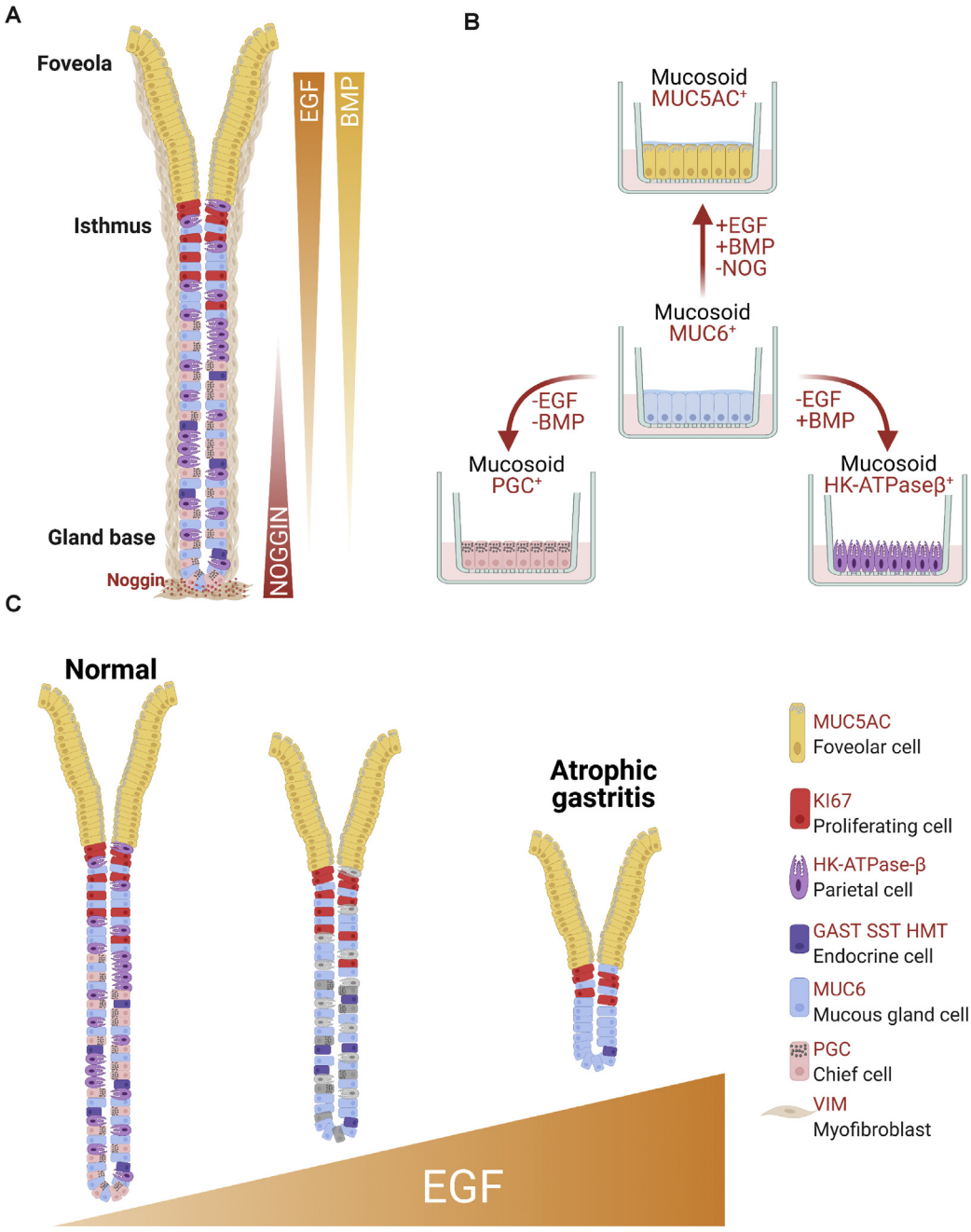

Figure 7. A new map of the human gastric gland. (*A*) A schematic of the human gastric gland showing the positions of the different cells and of the differentiation factors EGF, BMP, and Noggin. (*B*) A diagram summarizing the combination of signaling factors required to obtain differentiated cell types in the mucosoids. (*C*) Elevated levels of EGF are detrimental for chief and parietal cells and are probably underlying the histologic condition of AG. Markers are listed in *pink* above the cell types.

mucosa, the level of *EGF* is not significantly different in CG compared to normal. As expected, the expression levels of *PGC* and *ATP4B* were reduced in AG compared to CG and normal, consistent with loss of parietal and chief cells (Figure 6*B* and *C*). Further, we found that higher *EGF* expression in a biopsy corresponded to lower expression of *PGC* and *ATP4B* (Figure 6*D* and *E*). We also found a minor increase in expression of another known EGFR ligand called amphiregulin (*AREG,* Figure 6*F*), whereas *TGFA* and *HBEGF* were down-regulated (Figure 6*G* and *H*). The expression level of *BMP4* was similar across the sample types, but there was a significantly lower level of *ID1* in AG (Figure 6*I* and *J*). Reduced expression of *ID1* could be the result of increased expression of Noggin, however, the transcript *NOG* could not be detected because it is expressed in the muscularis mucosa (Figure 2*F*), which is not included in the biopsy. These data suggest that the loss of chief and parietal cells observed in AG is due to the high activation of the EGFR signaling

pathway, probably by EGF, which we have shown to preclude the differentiation of those lineages.

Discussion

We harnessed the multilineage differentiation capacity of the recently established mucosoid culture system to understand the signaling microenvironment controlling cell differentiation in human gastric glands. Aided by staining on the tissue of origin, we have found that stomach lineage differentiation is controlled by a gradient of EGF and BMP from the top to the base of the gland; and Noggin expressed in the muscularis mucosa. In particular, EGF is essential for foveolar differentiation and detrimental for chief and parietal cell differentiation. BMP pathway activation is found concomitant with foveolar differentiation, whereas Noggin (a BMP signaling inhibitor) blocks this lineage. We also found that activation of BMP signaling in the absence of active EGF induces parietal cell differentiation, while repressing chief cell differentiation (Figure 7*A* and *B*).

Homeostasis of glands depends on the capacity of cells to regenerate and differentiate into different lineages. Regeneration and the origin of lineages have been investigated extensively, especially in murine models. Although there is not yet a consensus on the "identity" of stem cells in the stomach,[4,31–37] it is evident that activation of the Wnt/β-catenin signaling pathway is essential for regeneration.[4–7] However, we and others have demonstrated that deactivation of this pathway induces foveolar cell differentiation specifically.[5,7] Other cell types, like chief and parietal cells, do not automatically differentiate, and they require different sets of instructions. Here we report that cellular differentiation in the glands is an active process driven by EGF and BMP/Noggin signaling, and we propose a model in which the signaling microenvironment is important in epithelial homeostasis, as it governs differentiation and patterning of human gastric glands. Indeed, we predict that an alteration in the signaling microenvironment, like the high expression of EGF found in Atrophic gastritis (AG), is the main driver of the histologic phenotype (lack of chief and parietal cells) observed in this precancerous condition.

Perturbation of EGF signaling is often associated with pathologic conditions, including gastric cancer. Long-term infection with *H. pylori* is a major risk for the development of gastric cancer,[38] and it is known that this bacterium is able to induce transactivation of the EGFR in epithelial cells,[39–41] probably as a response to extensive cell damage.[42] Gastric cancer initiates through a series of pathologically defined stages and AG is the first recognized precancerous condition, conferring a significantly higher chance of developing adenocarcinoma.[43] The altered mucosal morphology in AG may be due to the extensive damage caused by the infection. By enhancing cell proliferation, activation of EGFR might be needed to repair the damage. Previous reports have described the overexpression of EGFR ligands like TGFα, heparin-binding EGF, and amphiregulin in gastric cancer and also specifically in AG.[44] We propose that high expression of EGF prevents differentiation of functional chief and parietal cells in AG (Figure 7*C*). Furthermore, our findings show that EGF might predict the local severity of AG, as higher EGF correlates with fewer parietal and chief cells. Our findings are also consistent with studies of parietal cells isolated from rabbit, pig, and rat, demonstrating a role for EGFR activation in the inhibition of acid production.[45,46]

Several researchers have hypothesized that BMP might be the counter-effector of Wnt signaling in the mouse stomach mucosa.[18,47,48] Interestingly, transgenic mouse models overexpressing Noggin under the promoter of the proton pump lose mucin staining at the tip of the glands,[18] suggesting that this factor is detrimental to MUC5AC expression; our model is in line with this hypothesis. However, the BMP/Noggin circuit is not sufficient to segregate foveolar cells from the rest of the gland in the stomach, and we found that EGF is located at the foveolae and is indispensable for cell fate decisions. The role of EGFR activation in promoting foveolar cell differentiation is also consistent with the foveolar hyperplasia observed in Menetrier disease.[49,50] In this rare, premalignant condition, overexpression of TGFα (another EGFR activator) induces hyperproliferation of foveolar cells and excessive secretion of gastric mucus that can be reverted by blocking EGFR.[51,52]

Activation of EGFR by EGF is probably the main microenvironmental instruction dictating shape and cell content in the human stomach, and its effect may be similar in the rest of the gastrointestinal tract.

Supplementary Material

Note: To access the supplementary material accompanying this article, visit the online version of *Gastroenterology* at www.gastrojournal.org, and at http://doi.org/10.1053/j.gastro.2021.04.062.

References

1. Nordman H, Davies JR, Lindell G, et al. Gastric MUC5AC and MUC6 are large oligomeric mucins that differ in size, glycosylation and tissue distribution. Biochem J 2002; 364:191–200.
2. Seidlitz T, Koo BK, Stange DE. Gastric organoids-an in vitro model system for the study of gastric development and road to personalized medicine. Cell Death Differ 2021;28:68–83.
3. Burclaff J, Willet SG, Saenz JB, et al. Proliferation and differentiation of gastric mucous neck and chief cells during homeostasis and injury-induced metaplasia. Gastroenterology 2020;158:598–609.e5.
4. Barker N, Huch M, Kujala P, et al. Lgr5(+ve) stem cells drive self-renewal in the stomach and build long-lived gastric units in vitro. Cell Stem Cell 2010;6:25–36.
5. Bartfeld S, Bayram T, van de Wetering M, et al. In vitro expansion of human gastric epithelial stem cells and their responses to bacterial infection. Gastroenterology 2015; 148:126–136.e6.
6. Schlaermann P, Toelle B, Berger H, et al. A novel human gastric primary cell culture system for modelling *Helicobacter pylori* infection in vitro. Gut 2016;65:202–213.

7. Boccellato F, Woelffling S, Imai-Matsushima A, et al. Polarised epithelial monolayers of the gastric mucosa reveal insights into mucosal homeostasis and defence against infection. Gut 2019;68:400–413.
8. Lancaster MA, Huch M. Disease modelling in human organoids. Dis Model Mech 2019;12.
9. Clevers H. Modeling development and disease with organoids. Cell 2016;165:1586–1597.
10. Bartfeld S. Modeling infectious diseases and host-microbe interactions in gastrointestinal organoids. Dev Biol 2016;420:262–270.
11. McCracken KW, Cata EM, Crawford CM, et al. Modelling human development and disease in pluripotent stem-cell-derived gastric organoids. Nature 2014;516:400–404.
12. Choi E, Roland JT, Barlow BJ, et al. Cell lineage distribution atlas of the human stomach reveals heterogeneous gland populations in the gastric antrum. Gut 2014;63:1711–1720.
13. Houweling AC, Dildrop R, Peters T, et al. Gene and cluster-specific expression of the Iroquois family members during mouse development. Mech Dev 2001;107:169–174.
14. McCracken KW, Aihara E, Martin B, et al. Wnt/beta-catenin promotes gastric fundus specification in mice and humans. Nature 2017;541:182–187.
15. Nookaew I, Thorell K, Worah K, et al. Transcriptome signatures in *Helicobacter pylori*-infected mucosa identifies acidic mammalian chitinase loss as a corpus atrophy marker. BMC Med Genom 2013;6:41.
16. Mah AT, Yan KS, Kuo CJ. Wnt pathway regulation of intestinal stem cells. J Physiol 2016;594:4837–4847.
17. Fischer AS, Sigal M. The role of Wnt and R-spondin in the stomach during health and disease. Biomedicines 2019;7.
18. Shinohara M, Mao M, Keeley TM, et al. Bone morphogenetic protein signaling regulates gastric epithelial cell development and proliferation in mice. Gastroenterology 2010;139:2050–2060.e2.
19. Gehart H, Clevers H. Tales from the crypt: new insights into intestinal stem cells. Nat Rev Gastroenterol Hepatol 2019;16:19–34.
20. He XC, Zhang J, Tong W-G, et al. BMP signaling inhibits intestinal stem cell self-renewal through suppression of Wnt–β-catenin signaling. Nat Genet 2004;36:1117–1121.
21. Kosinski C, Li VSW, Chan ASY, et al. Gene expression patterns of human colon tops and basal crypts and BMP antagonists as intestinal stem cell niche factors. Proc Natl Acad Sci U S A 2007;104:15418–15423.
22. Stzepourginski I, Nigro G, Jacob J-M, et al. CD34 + mesenchymal cells are a major component of the intestinal stem cells niche at homeostasis and after injury. Proc Natl Acad Sci U S A 2017;114:E506–E513.
23. Choi E, Means AL, Coffey RJ, et al. Active Kras expression in gastric isthmal progenitor cells induces foveolar hyperplasia but not metaplasia. Cell Mol Gastroenterol Hepatol 2019;7:251–253.e1.
24. Goldenring JR, Ray GS, Soroka CJ, et al. Overexpression of transforming growth factor-alpha alters differentiation of gastric cell lineages. Dig Dis Sci 1996;41:773–784.
25. Tremblay E, Monfils S, Menard D. Epidermal growth factor influences cell proliferation, glycoproteins, and lipase activity in human fetal stomach. Gastroenterology 1997;112:1188–1196.
26. Fukuyama R, Shimizu N. Expression of epidermal growth factor (EGF) and the EGF receptor in human tissues. J Exp Zool 1991;258:336–343.
27. Romrell LJ, Coppe MR, Munro DR, et al. Isolation and separation of highly enriched fractions of viable mouse gastric parietal cells by velocity sedimentation. J Cell Biol 1975;65:428–438.
28. Zhou R, Zhu L, Kodani A, et al. Phosphorylation of ezrin on threonine 567 produces a change in secretory phenotype and repolarizes the gastric parietal cell. J Cell Sci 2005;118:4381–4391.
29. Lennerz JK, Kim SH, Oates EL, et al. The transcription factor MIST1 is a novel human gastric chief cell marker whose expression is lost in metaplasia, dysplasia, and carcinoma. Am J Pathol 2010;177:1514–1533.
30. Link A, Schirrmeister W, Langner C, et al. Differential expression of microRNAs in preneoplastic gastric mucosa. Sci Rep 2015;5:8270.
31. Hayakawa Y, Ariyama H, Stancikova J, et al. Mist1 expressing gastric stem cells maintain the normal and neoplastic gastric epithelium and are supported by a perivascular stem cell niche. Cancer Cell 2015;28:800–814.
32. Choi E, Lantz TL, Vlacich G, et al. Lrig1+ gastric isthmal progenitor cells restore normal gastric lineage cells during damage recovery in adult mouse stomach. Gut 2018;67:1595–1605.
33. Han S, Fink J, Jorg DJ, et al. Defining the identity and dynamics of adult gastric isthmus stem cells. Cell Stem Cell 2019;25:342–356.e7.
34. Stange DE, Koo BK, Huch M, et al. Differentiated Troy+ chief cells act as reserve stem cells to generate all lineages of the stomach epithelium. Cell 2013;155:357–368.
35. Arnold K, Sarkar A, Yram MA, et al. Sox2(+) adult stem and progenitor cells are important for tissue regeneration and survival of mice. Cell Stem Cell 2011;9:317–329.
36. Yoshioka T, Fukuda A, Araki O, et al. Bmi1 marks gastric stem cells located in the isthmus in mice. J Pathol 2019;248:179–190.
37. Tan SH, Swathi Y, Tan S, et al. AQP5 enriches for stem cells and cancer origins in the distal stomach. Nature 2020;578:437–443.
38. Traulsen J, Zagami C, Daddi AA, et al. Molecular modelling of the gastric barrier response, from infection to carcinogenesis [published online ahead of print February 22, 2021]. Best Pract Res Clin Gastroenterol doi:10.1016/j.bpg.2021.101737
39. Keates S, Keates AC, Katchar K, et al. Helicobacter pylori induces up-regulation of the epidermal growth factor receptor in AGS gastric epithelial cells. J Infect Dis 2007;196:95–103.

40. Keates S, Keates AC, Nath S, et al. Transactivation of the epidermal growth factor receptor by cag+ *Helicobacter pylori* induces upregulation of the early growth response gene Egr-1 in gastric epithelial cells. Gut 2005;54:1363–1369.
41. Romano M, Ricci V, Di Popolo A, et al. *Helicobacter pylori* upregulates expression of epidermal growth factor-related peptides, but inhibits their proliferative effect in MKN 28 gastric mucosal cells. J Clin Invest 1998;101:1604–1613.
42. Yan F, Cao H, Chaturvedi R, et al. Epidermal growth factor receptor activation protects gastric epithelial cells from Helicobacter pylori-induced apoptosis. Gastroenterology 2009;136:1297–1307; e1–e33.
43. Whiting JL, Sigurdsson A, Rowlands DC, et al. The long term results of endoscopic surveillance of premalignant gastric lesions. Gut 2002;50:378–381.
44. Schiemann U, Konturek J, Assert R, et al. mRNA expression of EGF receptor ligands in atrophic gastritis before and after *Helicobacter pylori* eradication. Med Sci Monit 2002;8:Cr53–Cr58.
45. Engevik AC, Kaji I, Goldenring JR. The physiology of the gastric parietal cell. Physiol Rev 2020;100:573–602.
46. Nitsche H, Ramamoorthy S, Sareban M, et al. Functional role of bone morphogenetic protein-4 in isolated canine parietal cells. Am J Physiol Gastrointest Liver Physiol 2007;293:G607–G614.
47. Bartfeld S, Koo BK. Adult gastric stem cells and their niches. Wiley Interdiscip Rev Dev Biol 2017;6(2).
48. Ye W, Takabayashi H, Yang Y, et al. Regulation of gastric Lgr5+ve cell homeostasis by bone morphogenetic protein (BMP) signaling and inflammatory stimuli. Cell Mol Gastroenterol Hepatol 2018;5:523–538.
49. Coffey RJ, Washington MK, Corless CL, et al. Menetrier disease and gastrointestinal stromal tumors: hyperproliferative disorders of the stomach. J Clin Invest 2007;117:70–80.
50. Huh WJ, Coffey RJ, Washington MK. Menetrier's disease: its mimickers and pathogenesis. J Pathol Transl Med 2016;50:10–16.
51. Settle SH, Washington K, Lind C, et al. Chronic treatment of Menetrier's disease with Erbitux: clinical efficacy and insight into pathophysiology. Clin Gastroenterol Hepatol 2005;3:654–659.
52. Nomura S, Settle SH, Leys CM, et al. Evidence for repatterning of the gastric fundic epithelium associated with Menetrier's disease and TGFalpha overexpression. Gastroenterology 2005;128:1292–1305.

Received February 26, 2020. Accepted April 24, 2021.

Correspondence
Address correspondence to: Thomas F. Meyer PhD, Department of Molecular Biology, Max Planck Institute for Infection Biology, Berlin, 10117, Germany. e-mail: meyer@mpiib-berlin.mpg.de; or Francesco Boccellato PhD, Ludwig Institute for Cancer Research, Nuffield Department of Clinical Medicine, University of Oxford, Oxford OX3 7DQ, United Kingdom. e-mail: francesco.boccellato@ludwig.ox.ac.uk.

Acknowledgments
The authors acknowledge Mary Muers (Ludwig Institute for Cancer Research, University of Oxford, UK) for editing the manuscript. We thank Dagmar Frahm (Max Planck Institute for Infection Biology, Berlin, Germany) and Cosima Thon (Department of Gastroenterology, Hepatology and Infectious Diseases, Magdeburg, Germany) for the support with mucosoid cultures and the gastric biopsies and Hans J. Mollenkopf and Ina Wagner (Max Planck Institute for Infection Biology, Berlin, Germany) for the microarrays. Illustrations were made using biorender.com. This study was partially funded by the COVID-19 Rebuilding Research Momentum Fund (BRD00230), Medical Science Division, University of Oxford. Transcript profiling: Microarray data have been deposited in the Gene Expression Omnibus (GEO; www.ncbi.nlm.nih.gov/geo/) of the National Center for Biotechnology Information and can be accessed with the GEO accession number GSE141660. Alice Anna Daddi, Aki Imai-Matsushima, and Kristin Fritsche contributed equally to this work.

CRediT Authorship Contributions
Sarah Wölffling, PhD (Data curation: Lead; Investigation: Lead; Methodology: Lead; Validation: Lead; Visualization: Lead).
Alice Anna Daddi BSc (Investigation: Supporting). Aki Imai-Matsushima, MD (initiation of the project: Equal).
Kristin Fritsche, PhD (Data curation: Equal; Formal analysis: Equal).
Christian Goosmann, PhD (Data curation: Equal; Formal analysis: Equal; Methodology: Equal).
Jan Traulsen, MSc (Investigation: Supporting).
Richard Lisle, PhD (Methodology: Supporting).
Monika Schmid, PhD (Data curation: Equal; Methodology: Equal).
Maria del Mar Reines-Benassar, PhD (initiation of the project: Supporting).
Lennart Pfannkuch, MD (initiation of the project: Supporting).
Jan Bornschein, MD (provision of human tissue samples: Equal).
Peter Malfertheiner, MD (Funding acquisition: Supporting; provision of human tissue samples: Equal).
Jürgen Ordemann, MD (provision of human tissue samples: Lead).
Alexander Link, MD (provision of human tissue samples: Lead).
Thomas F. Meyer, PhD (Conceptualization: Equal; Funding acquisition: Lead; Project administration: Lead; Supervision: Lead; Writing – review & editing: Equal; Head of Department: Lead).
Francesco Boccellato, PhD (Conceptualization: Lead; Data curation: Lead; Formal analysis: Lead; Investigation: Lead; Methodology: Lead; Supervision: Lead; Writing – original draft: Lead; Writing – review & editing: Lead).

Conflicts of interest
The authors disclose no conflicts.

Funding
The clinical study and the collection of biopsies was supported by funds from BMBF No. BMBF-0315905D in the frame of an ERA-NET PathoGenoMics project.

Supplementary Material and Methods

Human Tissue

Gastric sleeve resections were provided by the Centre for Obesity and Metabolic Medicine, Helios Klinikum, (Berlin-Buch, Germany) with prior approval of the ethics committee of the Charité University Hospital, Berlin (EA1/129/12). Every participant provided his written informed consent before study inclusion. Anonymized samples (Supplementary Table 1) were obtained from a total of 11 patients with body mass index >36 kg/m^2. The tissue was washed in phosphate-buffered saline (PBS) containing 50 μg/mL gentamicin to remove blood and then processed by removing fat and connective tissue. A 2 × 2 cm^2 portion of tissue was taken from the central part of the corpus and from the antrum. The tissue was further divided for generating samples for histology and for cell isolation, and the rest was snap-frozen. In addition, gastric biopsies were collected from patients undergoing upper gastrointestinal endoscopy at the Department of Gastroenterology, Hepatology and Infectious Diseases at the Otto-von-Guericke University Magdeburg, Germany (Supplementary Table 3). The study protocol was approved by the Institutional Review Board of Otto-von-Guericke University Magdeburg (ethics reference 80/11). The detailed study design was described previously.[1] Briefly, every participant provided written informed consent before study inclusion. A pair of biopsies was immediately snap-frozen in liquid nitrogen and stored at −80°C until further processing and extraction of nucleic acids. Additional biopsies from the gastric antrum, the incisura angularis, and the gastric corpus were processed for routine histopathology assessment according to the updated Sydney classification.[2] This includes grading of the activity of the mucosal inflammation by assessment of the infiltration by neutrophil granulocytes and the chronicity of inflammation by assessment of the infiltration by lymphocytes accordingly. The degree of mucosal atrophy was defined by the structural reduction of the mucosal gland architecture, and the degree of intestinal metaplasia by the extent of intestinalized glands within the samples.[2] Based on these results, patients were stratified into the following groups: AG, in case of significant atrophic changes (the degree of intestinal metaplasia was not included in this definition); CG, in case of inflammatory but no structural changes of the mucosa; and normal, in the absence of relevant inflammation and structural changes. Patients in the AG group were also stratified according to the Operative Link on Gastritis Assessment and Operative Link on Gastric Intestinal Metaplasia Assessment stages, as described previously.[3,4] According to the updated Sydney system, *Helicobacter pylori* density was assessed by histopathology. Status of *H pylori* infection was determined by rapid urease test and microbiology (culture), as well as serology. Patients were defined as *H. pylori*–positive with positive microbiology and/or positive histology and/or positive serology. Positive serology only indicates past rather than active infection. Patients negative in these modalities were defined as *H. pylori*–negative. In the experimental part of this study, only biopsies from the corpus were used.

Generation of the Mucosoids

Gastric tissue from sleeve resections was processed as described previously.[6] The tissue (0.5–1 cm^2) from antrum and from corpus was cut into pieces <1 mm^2 and washed in cold PBS until the supernatant was clear (8–10 times), followed by a 30-minute incubation in chelating solution (5.6 mM Na_2HPO_4/8.0 mM KH_2PO_4/96.2 mM NaCl/1.6 mM KCl/43.4 mM sucrose/54.9 mM D-sorbitol/0.5 mM DL-dithiothreitol/2 mM EDTA in H_2O) at 37°C on a shaking platform. Settled tissue fragments were transferred to a Petri dish and subjected to gentle pressure under a glass slide to extract the glands. The extracted portions of tissue were re-suspended in medium containing 10% heat-inactivated fetal calf serum (Biochrom) to reduce cell re-aggregation. After settling the larger fragment for 1 minute, the solution with the isolated glands was transferred into a new tube, centrifuged at 250*g* for 5 minutes and re-suspended in 600 μL of Matrigel (356231; Corning), and aliquoted in 50-μL drops in each well of a 24-well plate. The cell aggregates were cultivated to form organoids, according to a protocol published previously.[5] The organoids were cultivated for 2 passages before seeding them into mucosoids using a method established previously.[7] Briefly, 250,000 cells derived from either antrum or corpus organoids were seeded in 200 μL culture medium into collagen-coated (A10644-0, 12.5–15 μg/cm^2; Gibco) Transwell inserts (PIHP01250; Millipore) placed in a 24-well plate at 37°C, 5% CO_2 in a humidified incubator. The space between filter and well was filled with 400 μL culture medium (Supplementary Table 2). At day 3 post seeding, the medium overlying the cells was removed from the well insert to start the air–liquid interface culture. Subsequently the 500 μL medium below the filter was replaced twice a week. After 13 days, only half of the medium volume was changed regularly to maintain cell-secreted factors in the medium. Every 30–45 days, the mucosoids were expanded; top and bottom of inserts were washed 3 times with PBS, followed by 30–60 minutes of incubation with 0.05% trypsin/EDTA (25300; Thermo Scientific) on both sides of the filter. Cells were harvested, washed, and reseeded at 250,000 cells per new filter.

WNT3A- and RSPO1-Conditioned Media

WNT3A- and RSPO1-conditioned supernatants were produced using the cell lines L Wnt-3A and 293T Ha Rspo1 Fc 3/3, respectively. To measure the activity of WNT3A and RSPO1, 239T cells transfected with a vector containing 7 TCF/LEF binding sites driving the expression of GFP were used as reporter. Cells were seeded on poly-L-lysine–coated 96-well plates and exposed for 24 hours to different concentrations of both conditioned supernatants. Cells were then stained with Hoechst 33342 (1:1000; Invitrogen) and fixed with 4% paraformaldehyde for 30 minutes in the dark at room temperature (RT). The activity of WNT3A and RSPO1 supernatants was determined automatically from

images acquired with the Operetta High Content Imaging System (PerkinElmer), dividing the number of green "activated" cells by the total number of nuclei. Different lots of WNT3A-conditioned media were used only if 20%–25% of the conditioned medium diluted in Dulbecco's modified Eagle medium activated 50% of the test cells. Similarly, lots of RSPO1 were used only if 5%–10% of 293T Ha Rspo1 Fc 3/3–conditioned medium activated 50% of the test cells (5% of WNT3A-conditioned medium was used as a co-activator in the RSPO1 test).

Transmission Electron Microscopy and Immunogold Labeling

Resin sections. Mucosoid culture cells were fixed with 2.5% glutaraldehyde in PBS and post-fixed with 0.5% osmium-tetroxide, contrasted with uranyl-acetate and tannic acid, dehydrated in a graded ethanol series, and infiltrated in Polybed (Polysciences). Cut out pieces of the filters were stacked in flat embedding molds with Polybed. After polymerization, specimens were cut at 60 nm and contrasted with lead citrate. Specimens were analyzed in a Leo 906E transmission electron microscope (Zeiss, Oberkochen, Germany) equipped with a side-mounted digital camera (Morada; SIS-Olympus, Münster, Germany).

Cryosection Immunogold labeling. Mucosoid culture samples were fixed with 4% paraformaldehyde and 0.05% glutaraldehyde in PBS and filter membrane was cut into 1-mm-wide streaks. The filter membrane pieces were gelatin-embedded and infiltrated with 2.3M sucrose according to the method described previously.[5] Ultrathin sections were cut at −95°C with an RMC MTX/CRX cryo-ultramicrotome (Boeckeler Instruments Inc, Tucson, AZ) transferred to carbon- and pioloform-coated electron microscopy grids and blocked with 0.3% bovine serum albumin, 0.01 M glycin, 3% CWFG in PBS. The sections were incubated with appropriate dilutions in the same buffer of rabbit polyclonal antibody directed against PGC (Supplementary Table 4) or mouse antibody directed against HK-ATPase-β (Supplementary Table 4). Secondary antibody incubations were carried out with goat-anti-rabbit (or mouse) antibodies coupled to 12 nm gold particles (Jackson Immuno Research, West Grove, PA). Specimens were then contrasted and embedded with uranyl-acetate/methyl-cellulose following the method described previousy[6] and analyzed in a Leo 912AB transmission electron microscope (Zeiss, Oberkochen, Germany) at 120 kV acceleration voltage. Micrograph-mosaics were scanned using a bottom-mount Cantega digital camera (SIS, Münster, Germany) with ImageSP software from TRS (Tröndle, Moorenweis, Germany). Annotation of gold particles was performed with Fiji Image J[7,8] software using the "Gold Digger" macro.[9]

RNA isolation and quantitative real-time polymerase chain reaction analysis. Filters were cut from the insert and transferred in 1 mL Trizol (Thermo). After vigorous vortexing, the samples were incubated for 10 minutes at RT, and vortexed again before being frozen at −80°C. After 24 hours, samples were thawed, vortexed, and a volume of 500 μL chloroform was added. Samples were incubated for 2 minutes at RT and centrifuged for 15 minutes at 4°C. The aqueous phase was mixed with isopropanol, inverted 6 times, and incubated for 10 minutes at RT. The resulting sample was transferred to a Total RNA Isolation Kit Column (Thermo) and processed according to the manufacturer's instructions. Total RNA was measured using a NanoDrop and reverse transcription carried out using the Tetro cDNA synthesis Kit (Bioline). Quantitative real-time polymerase chain reaction (Step One; Applied Biosystem) was performed using the SensiMix SYBR hi-ROX Kit (Bioline). Primers are listed in Supplementary Table 5.

Histology

Histologic samples of the antrum or corpus were fixed overnight in 4% paraformaldehyde. Mucosoids on the filters were fixed overnight in 4% paraformaldehyde at 4°C or for 2 hours at room temperature, washed, embedded orthogonally in 0.5 mL Histogel (HG-4000-144) inside a casting mold. The gel block containing the mucosoid and the tissue where both paraffinized overnight in a TP1020 tissue processor (Leica). Paraffin blocks were cut into 5-μm sections with a paraffin rotation microtome (Microm). For dewaxing and antigen retrieval, sample slides were washed twice with Xylene (10 minutes), followed by a descending series of alcohols (20 seconds each), followed by 2 washes in running water (5 minutes) and 30 minutes in target retrieval solution (Dako) at 95°C. Samples were cooled down for 20 minutes at RT and washed 5 minutes under running water. For whole-mount samples, the filters were fixed for 20 minutes in 4% paraformaldehyde at 37°C and washed with PBS. Samples were optionally incubated for 10 minutes in methanol at −20°C to increase the permeability of the sample to antibodies against nuclear proteins. The samples (both whole mount or sections on glass slides) were rehydrated in PBS and incubated with blocking solution (PBS, 1% bovine serum albumin, 2% fetal calf serum or PBS, 5% donkey serum, 0.3% Triton X-100 for MUC5AC and MUC6 staining) for 1 hour, followed by primary antibody (in blocking solution) for 90 minutes at RT. After 3 washes with PBS + 0.1% Tween, samples were incubated with fluorescently labeled secondary antibodies and 4′,6-diamidino-2-phenylindole (1:1000) or Hoechst 33342 (1:1000; Invitrogen) and Alexa Fluor 647 Phalloidin (1:40; Thermo Fisher Scientific) for 120 minutes in the dark at RT. The antibodies are listed in Supplementary Table 4. Samples were washed 3 times with PBS, mounted in Mowiol, and analyzed by confocal microscopy using a Leica TCS SP-8 microscope or a Zeiss LSM 710. Images were processed, analyzed with ImageJ and QuPath, and imported into Adobe Illustrator for labeling.

Analysis of Epidermal Growth Factor Staining on Human Sections

The images were processed with the software ZEN, version 2.3 (blue edition) and Fiji ImageJ. The latter was used to measure the average intensity of EGF signal of the whole image and per defined region. The glands from 4 sections of 2 different samples were stained, imaged,

aligned, and divided in 10 regions of interest (ROIs) numbered from top to bottom. The height of each ROI is approximately 55 μm. Mean intensity of signals was measured in each ROI and the percentage in each ROIs was calculated. The mean ± SD of the percentage of each ROI from 4 sections of 2 different samples is plotted next to the picture. Statistical analysis was performed and ordinary 1-way analysis of variance (ANOVA). Distribution of the signal between ROIs was statistically significant from a random distribution ($P < .05$). A Tukey's multiple comparison test after the ANOVA revealed that values of ROI 1 in the staining are significantly different ($P < .05$) compared to the signals of all other ROIs (but not ROI 2).

Hematoxylin Staining

Paraffin-embedded samples were deparaffinized using Histo-Clear II (HS-202; National Diagnostics) and rehydrated by stepwise incubation in 100%, 90%, and 70% ethanol. Samples were stained for 5 minutes in Harris hematoxylin (HHS32; Sigma Aldrich), washed 10 times, briefly differentiated in acidic ethanol (1% 1M HCl in 70% ethanol), and blued for 30 seconds in tap water. Samples were dehydrated by stepwise incubation in 70%, 90%, and 100% ethanol and Histo-Clear II. Stained samples were mounted with VectaMount (H-5000; Vector Laboratories). Images were acquired using the Hamamatsu NanoZoomer S210 slide scanner.

RNA Scope

For the in situ hybridization, the RNAScope 2.5 HD Reagent Kit-RED from ACD was used following the supplier's protocol, while the incubation time in "target retrieval reagent," peroxidase and AMP5 were adapted to the tissue. In brief, slides were baked in a dry oven at 60°C, 60 minutes followed by incubation in 2× 5 minutes in Xylene and 2× 2 minutes 100% ethanol at RT. After air drying, slides were incubated with RNAscope hydrogen peroxide (10 minutes, RT) and washed twice with distilled water. Slides were transferred to preheated 1× target retrieval reagent and boiled for 17 minutes at 98°C–102°C, followed by 5 minutes washing in distilled water and once in 100% ethanol. Dried slides were placed in a HybEZ slide rack and sections were incubated with RNAscope Protease Plus for 22 minutes at 40°C and washed twice for 2 minutes in distilled water. Prewarmed probe was hybridized to sample for 2 hours at 40°C. Slides were washed 2× 2 minutes in 1× wash buffer. Next, slides were incubated with AMP1 (30 minutes, 40°C), AMP2 (15 minutes, 40°C), AMP3 (30 minutes, 40°C), and AMP4 (15 minutes, 40°C). Between each AMP-step slides were washed with 1× wash buffer 2× 2 minutes. Then, slides were incubated with AMP5 for 45 minutes at RT, washed 2× 2 minutes in 1× wash buffer and incubated with AMP6 for 15 minutes at RT and finally washed 2× 2 minutes with 1× wash buffer. Sections were incubated for 10 minutes at RT with RED working solution. Next, slides were washed twice in distilled water. Sections were incubated in 50% hematoxylin for 5 minutes at RT, followed by washing in distilled water and short incubation in 0.02% ammonia water until sections turn blue. Sections were washed with water and dried at 60°C. Before mounting, sections were shortly dipped in fresh xylene and finally mounted with EcoMount. The purchased probes are listed in Supplementary Table 6.

Analysis of RNAscope Data

Images of the in situ hybridization samples were recorded with an Axion Scan.Z1 microscope (Zeiss) by the MPIIB core facility microscopy. The images were processed with the software ZEN, version 2.3 (blue edition) and Fiji ImageJ. The latter was used to count the number of signal spots of the whole image and per defined region. Therefore, the tools "colour deconvolution," "threshold," and "analyze particles" were used. The glands from different images were aligned and divided in 10 ROIs numbered from top to bottom. The height of each ROI is approximately 55 μm. Number of dots were counted in each ROI and calculated in percentage to all dots in all ROIs. The mean ± SD of the percentage of each ROI from 4 different pictures is plotted next to the graph. Statistical analysis was performed an ordinary 1-way ANOVA. Distribution of the signal between ROIs is statistically significant from a random distribution, $P < .05$) for BMP4, BMP2, EGF, and TGFα. It is not significant ($P = .25$ for the positive control RNAPOL2. A Tukey's multiple comparison test following the ANOVA revealed that values of ROI 3 in the stainings for BMP4, EGF, and TGFα are significantly different compared to the signals of other ROIs. Details of the Tukey's multiple comparison test: BMP4: ROI 3 vs ROI 1, 5, 6, 7, 9 ($P < .05$); BMP2: ROI 3 vs ROI 1, 5 ($P < .05$); EGF: ROI 3 vs ROI 5, 6, 7, 8, and 10 ($P < .05$); TGFα ROI 3 vs ROI 1, 4, 5, 6, 7, 8, 9, and 10 ($P < .05$). All other pairwise comparisons in the Tukey's test are not significant.

Monitor of Acid Production by Parietal Cells Using Acridine Orange

Two corpus mucosoid samples were taken at passage 4 in air–liquid interface and grown for 13 days in regular medium (Supplementary table 2), followed by 2 weeks' treatment with 50 ng/mL of BMP4 and removal of Noggin and EGF. The mucosoids were preincubated with 1 μm acridine orange for 15 minutes. The filter was cut out of the insert and mounted with the cells facing the glass of a μ-Dish chamber (cat #81158; IBIDI) with 400 μL of media (the same with acridine orange). A coverslip was put on top. Images were taken with 25× (glycerol) for 10 minutes to stabilize the filter and avoid movements A solution of 10 μL of 5 mM histamine in medium was applied to samples on the border of the coverslip while imaging. Fluorescence of acridine orange was excited at 488 nm (3%–4%) and images were collected in a time series (10 seconds) at 500–550 nm and 600–650 nm. Pinhole was opened at 180–190 AU. Images were analyzed by Fiji and corrected for (X–Y) drifts of the sample. Pictures were generated by averaging the signal from 9 time points (90 seconds). The background-corrected 500–550 nm/600–650 nm fluorescence emission ratio image was

calculated and normalized to a value of 1 baseline of the first pictures of the time series when no histamine was applied.

Microarray Analysis

Microarrays were hybridized for mucosoid cultures derived from 3 different patients cultured in +W+R or –W–R medium for 5 days followed by infection for 3 days in the same condition. Filters with mucosoid cultures were dissolved in 1 mL Trizol (Life Technologies) and RNA isolated per the manufacturer's protocol. Quantity of RNA was measured using NanoDrop 1000 UV-Vis spectrophotometer (Kisker) and quality was assessed by Agilent 2100 Bioanalyzer with an RNA Nano 6000 microfluidics kit (Agilent Technologies). Microarray experiments were performed as single-color hybridizations on custom whole genome human 8×60K Agilent arrays (Design ID 048908) according to the manufacturer's instructions and Agilent Feature Extraction software used to obtain probe intensities. The extracted single-color raw data files were background corrected, quantile normalized, and further analyzed for differential gene expression using R and the associated BioConductor package LIMMA.[2] Microarray gene expression comparisons between groups were performed using paired test between conditions. Microarray data have been deposited in the Gene Expression Omnibus (www.ncbi.nlm.nih.gov/geo/) of the National Center for Biotechnology Information and can be accessed with the Gene Expression Omnibus accession number GSE141660.

Mass Spectrometry Sample Preparation

The mucus samples were prepared according to the filter-aided sample preparation method[10] and following the modification published by Rodriguez-Pineiro et al.[11] Samples were diluted with 200 μL 6M guanidinium hydrochloride in 0.1M Tris/HCl pH 8.5 (GuHCl) and 5 nonhuman proteins (10 pmol/protein) were added to each sample as an internal control. After reducing cysteines by adding 30 μL 0.1M dithiothreitol and incubation at 60°C for 20 minutes, the samples were transferred into MRCF0R030 Microcon-30 kDa centrifugal filters and washed with 200 μL GuHCl. Alkylation was performed by adding 100 μL 0.05M iodoacetamide and incubation at RT for 20 minutes in the dark. After washing 2× with 100 μL GuHCl, followed by 2× 100 μL 50 mM ammonium bicarbonate/5% acetonitrile, the proteins were digested with 0.2 μg sequencing-grade modified trypsin (V5111; Promega) in 40 μL 50-mM ammonium bicarbonate/5% acetonitrile overnight at 37°C. Peptide mixtures were acidified with trifluoroacetic acid to 0.5% (vol/vol), desalted using ZipTip C18 (Millipore, 0.6-μL bed volume) and lyophilized.

Liquid Chromatography With Tandem Mass Spectrometry Analysis

The samples were analyzed using a QExactive Plus mass spectrometer (Thermo Fisher Scientific) coupled online to a Dionex UltiMate 3000 RSLCnano System (Thermo Fisher Scientific). After solubilization in 13 μL 2:98 (v/v) acetonitrile/water containing 0.1% trifluoroacetic acid, 10 μL of each sample was loaded on a C18 PepMap 100 trap column (300 μm × 5 mm; 5-μm particle size 100-Å pore size; Thermo Fisher Scientific) at a flow rate of 20 μL/min 2:98 (v/v) acetonitrile/water containing 0.1% trifluoroacetic acid for preconcentration and desalting. Separation was performed using an Acclaim C18 PepMap RSLC column (75 μm × 250 mm; 2-μm particle size 100-Å pore size; Thermo Fisher Scientific) at a flow rate of 300 nL/min. High-performance liquid chromatography solvent A was 0.1% (v/v) formic acid and peptides were eluted from the column using high-performance liquid chromatography solvent B 80:20 (v/v) acetonitrile/water containing 0.1% formic acid starting from 3%, increasing to 40 % in 85 minutes, and to 98% in 5 minutes. The peptides were analyzed in data-dependent acquisition mode that alternated between 1 mass spectrometry scan and 10 tandem mass spectrometry scans for the most abundant precursor ions. Mass spectrometry scans were acquired over a mass range of m/z 350–1600 and resolution was set to 70,000. Peptides were fragmented using higher-energy collisional dissociation at 27% normalized collision energy and measured in the orbitrap at a resolution of 17,500.

Protein Identification

Proteins were identified and quantified using the MaxQuant software (version 1.626) searching the SwissProt human sequence database (released 2018_11, 20412 entries). Searches were performed using the following parameters: max. Missed cleavages 2; variable modifications Oxidation (M); Acetyl (Protein N-term); pyro-Glu (Gln), and carbamidomethylation of cysteines as fixed modification. The false discovery rate was set to 0.01 for proteins, peptides, and modified sites. The full list of proteins detected in each condition analyzed is displayed in Supplementary Table 7.

Supplementary References

1. Link A, Langner C, Schirrmeister W, et al. *Helicobacter pylori* vacA genotype is a predominant determinant of immune response to *Helicobacter pylori* CagA. World J Gastroenterol 2017;23:4712–4723.
2. Dixon MF, Genta RM, Yardley JH, et al. Classification and grading of gastritis. The updated Sydney System. International Workshop on the Histopathology of Gastritis, Houston 1994. Am J Surg Pathol 1996; 20:1161–1181.
3. Rugge M, Genta RM. Staging gastritis: an international proposal. Gastroenterology 2005;129:1807–1808.
4. Capelle LG, de Vries AC, Haringsma J, et al. The staging of gastritis with the OLGA system by using intestinal metaplasia as an accurate alternative for atrophic gastritis. Gastrointest Endosc 2010;71:1150–1158.
5. Peters PJ, Bos E, Griekspoor A. Cryo-immunogold electron microscopy. Curr Protoc Cell Biol 2006. Chapter 4:Unit 4.7.

6. Slot JW, Geuze HJ, Gigengack S, et al. Immuno-localization of the insulin regulatable glucose transporter in brown adipose tissue of the rat. J Cell Biol 1991; 113:123–135.
7. Schindelin J, Arganda-Carreras I, Frise E, et al. Fiji: an open-source platform for biological-image analysis. Nat Methods 2012;9:676–682.
8. Schneider CA, Rasband WS, Eliceiri KW. NIH Image to ImageJ: 25 years of image analysis. Nat Methods 2012; 9:671–675.
9. Sjoliema KAS, Giepmans BNG. Automated annotating label in nanotomy. Microscopy Imaging Processing. Available at: https://analyticalscience.wiley.com/do/10.1002/imaging.5662. Published October 24, 2016. Accessed May 28, 2021.
10. Wisniewski JR, Zougman A, Nagaraj N, et al. Universal sample preparation method for proteome analysis. Nat Methods 2009;6:359–362.
11. Rodriguez-Pineiro AM, Bergstrom JH, Ermund A, et al. Studies of mucus in mouse stomach, small intestine, and colon. II. Gastrointestinal mucus proteome reveals Muc2 and Muc5ac accompanied by a set of core proteins. Am J Physiol Gastrointest Liver Physiol 2013; 305:G348–G356.

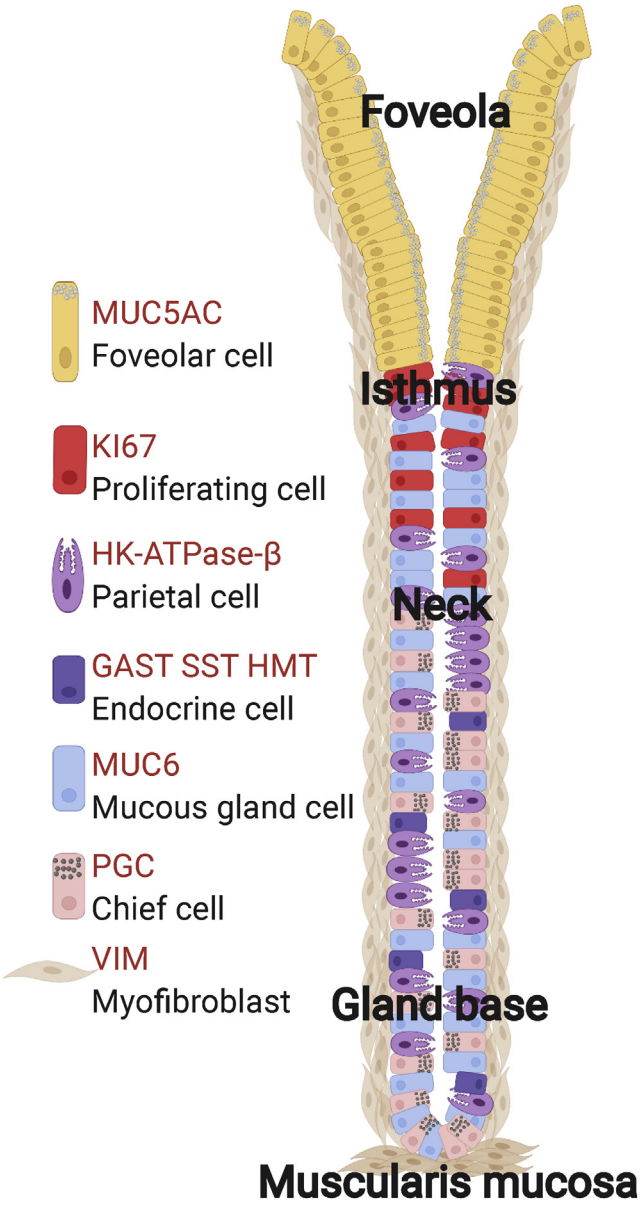

Supplementary Figure 1. Schematic of the human gastric gland in the corpus indicating the different regions and markers of the typical differentiated cell types.

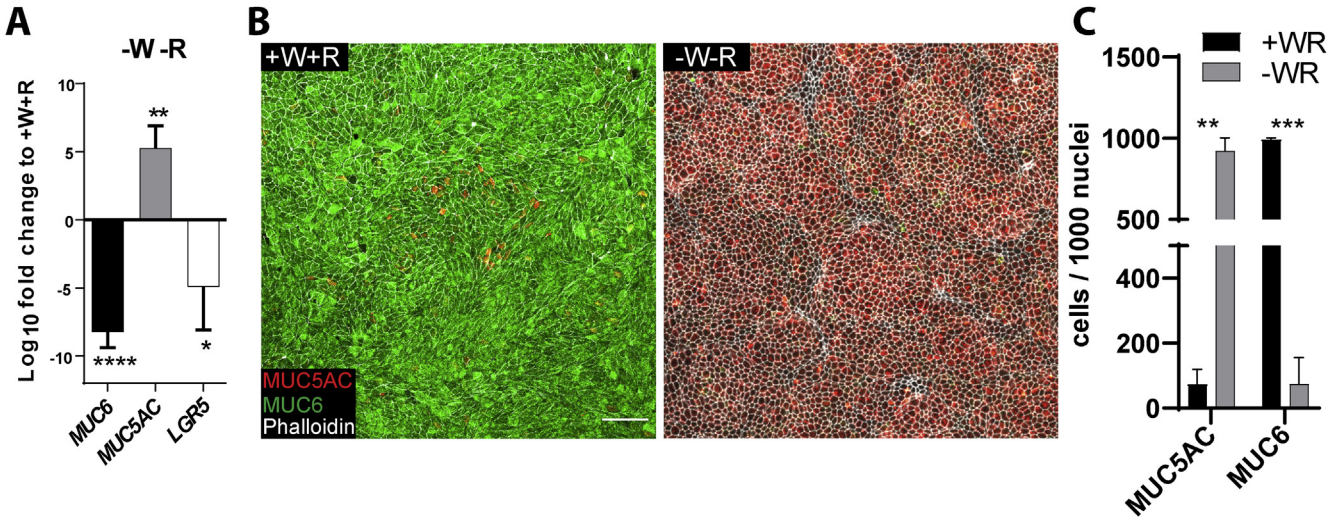

Supplementary Figure 2. Lack of WNT and RSPO promotes foveolar differentiation in corpus mucosoids. (*A*) Corpus mucosoids where depleted of WNT and RSPO from the cultivation media for 7 days and RNA was analyzed by quantitative real-time polymerase chain reaction analysis to detect *MUC5AC*, *MUC6*, and *LGR5* expression. Results are expressed in $\log_{10}$ fold-change relative to the +WNT +RSPO samples. (*B*) Immunofluorescence labeling against the foveolar marker MUC5AC shows that expression is low in the +W+R condition and increases after W/R are withdrawn for 12 days (–W–R). In contrast, expression of the basal marker MUC6 is high in the +W+R condition and reduces dramatically after W/R are withdrawn for 12 days. (*C*) Quantification (mean ± SD n = 4 biologic replicates) of MUC5AC and MUC6 cells in (*B*). *Scale bars:* 10 μm. (*A*, *C*) *t* test, **P* < .05; ***P* < .05; *****P* < .0005.

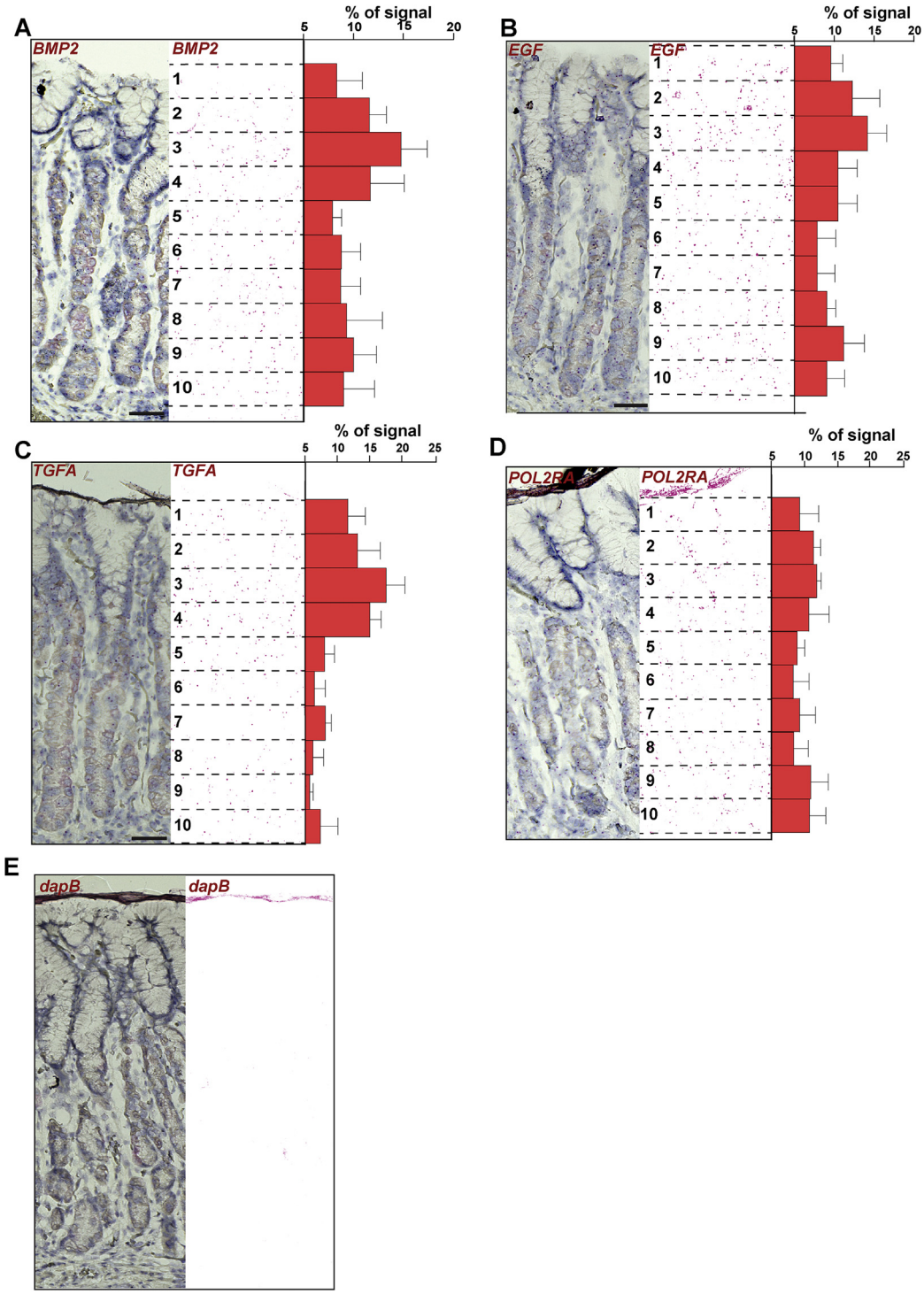

Supplementary Figure 3. Representative RNAscope in situ hybridization using probes detecting (*A*) *BMP2*, (*B*) *EGF*, (*C*) *TGFA*, (*D*) *POL2RA* (positive control), and (*E*) *DAPB* (negative control). The *left panels* show the RNAscope signals and hematoxylin counterstaining of human corpus gastric section. *Scale bar:* 50 μm. The *middle panels* show the RNA signal deconvolution (Supplementary Material) of the image of the *left panels*. The *right panels* show the quantification of the signal distribution from 4 or 5 aligned sections, divided in 10 ROIs (Supplementary Material). The distribution of the signals between the ROIs is statistically different from a random distribution for: BMP2, $P = .00170$; for EGF, $P < .0001$ and for TGFα, $P < .0001$ (1-way ANOVA). The distribution of the signals between the ROIs in the positive control (*POL2RA*) is not significantly different from a random distribution ($P = .025$, 1-way ANOVA).

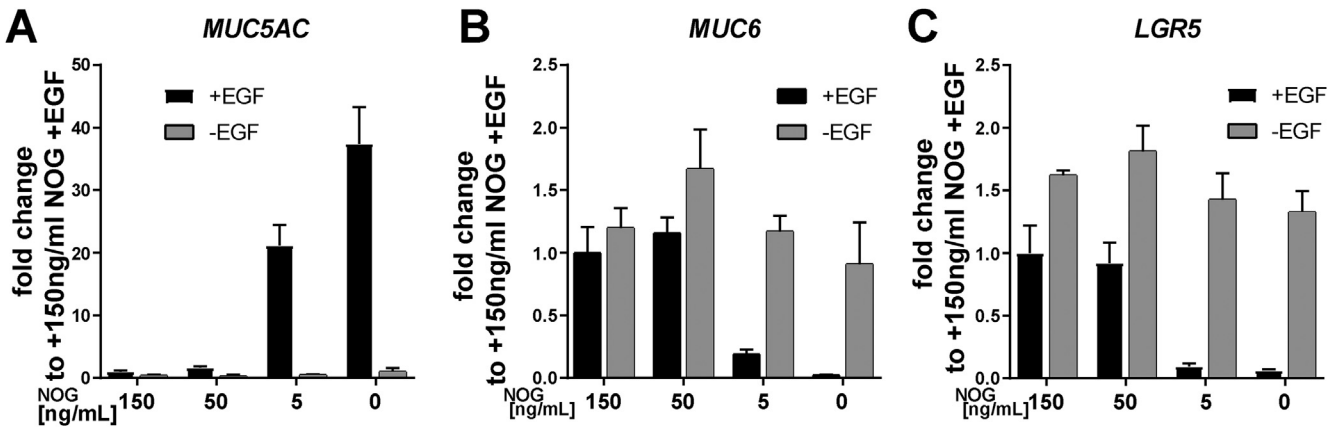

Supplementary Figure 4. Noggin preserves the MUC6^{+} neck cells from differentiation into foveolar cells. Titration of different concentrations of Noggin for 12 days in the presence or absence of EGF (20 ng/mL). Quantitative real-time polymerase chain reaction analysis of (*A*) *MUC5AC*, (*B*) *MUC6*, and (*C*) *LGR5*. Results are expressed in fold-change relative to the samples in the first column (150 ng/mL Noggin + EGF). Data represent technical triplicates of 1 sample set.

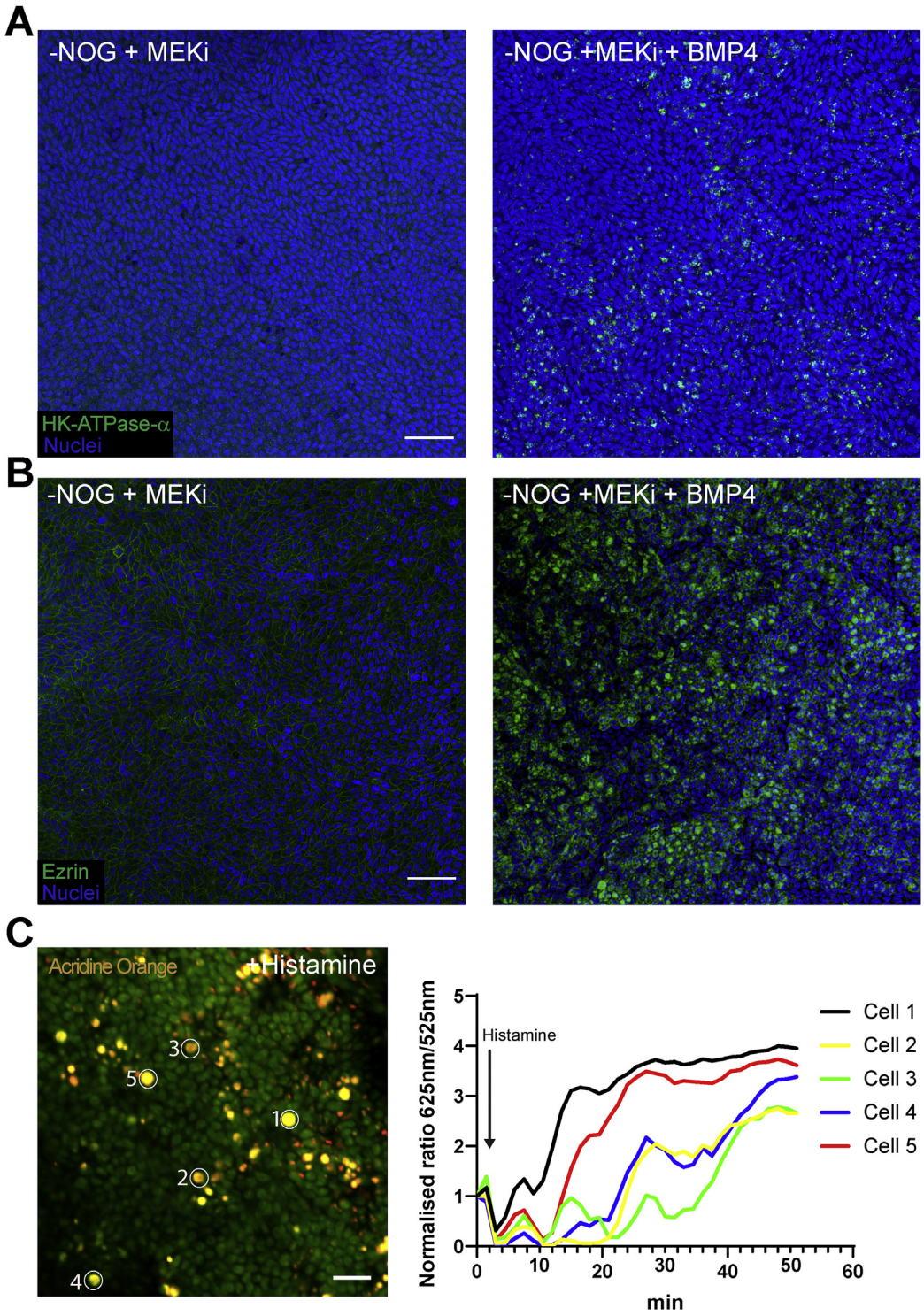

Supplementary Figure 5. Expression of HK-ATPase-α and Ezrin after BMP treatment. Mucosoids cultured –NOG + MEKi (2 μM) with or without BMP4 (50 ng/mL) treatment for 12 days were fixed and stained whole mount and visualized from top. (*A*) An anti–HK-ATPase-α antibody was used to confirm that the subunit α of the ATPase H+/K+ pump is induced by BMP4 (the subunit β is shown in Figure 5*E*). Nuclei were stained with Hoechst (in *blue*). *Scale bar:* 25 μm. (*B*) An anti-Ezrin antibody was used to stain membrane-cytoskeleton–associated structures. The staining shows an accumulation of signal on treatment with BMP, suggesting the formation of tubolovesicles typical of parietal cells (*green*). Nuclei were stained with Hoechst (in *blue*). *Scale bar:* 25 μm. (*C*) Mucosoids cultured –NOG + MEKi (2 μM) + BMP4 (50 ng/mL) for 12 days were treated with acridine orange and temporal changes in the ratio 625 nm/525 nm was measured (Supplementary Material) in response to histamine in 5 individual cells.

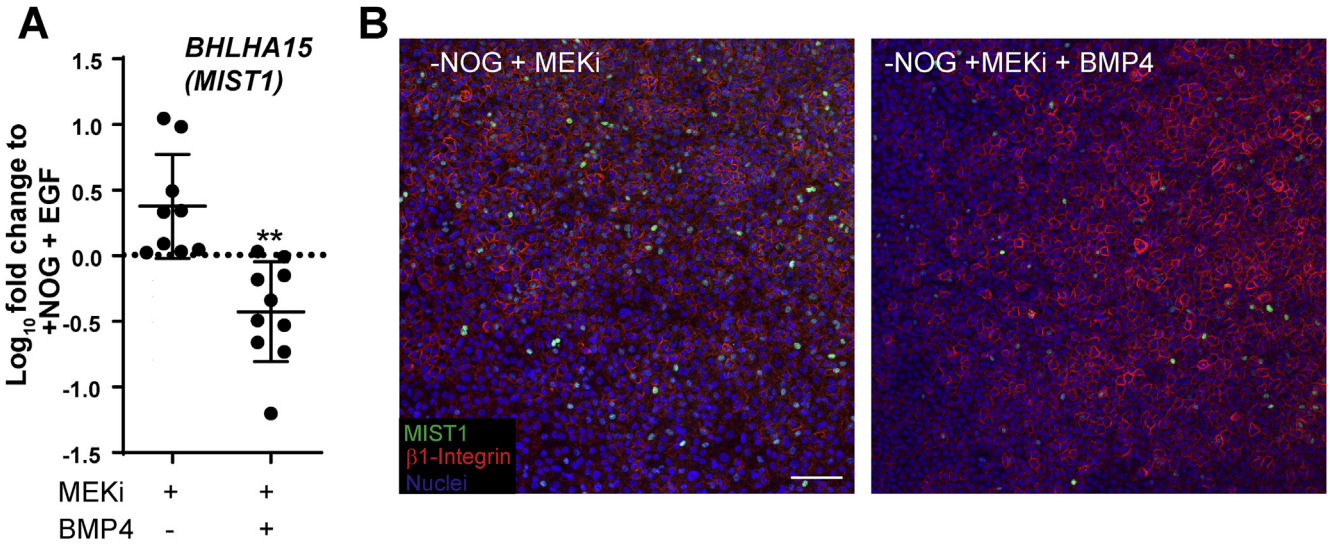

Supplementary Figure 6. Expression of MIST1 is reduced by BMP4. Mucosoids (–NOG +EGF) were treated with an inhibitor of MEK with or without BMP4 for 12 days. (*A*) Shown is quantitative real-time polymerase chain reaction for *MIST1*, expressed as log10 fold-change relative to +NOGGIN +EGF control samples. $^{**}P < .005$. (*B*) An anti-MIST1 antibody was used (*green*) for immunofluorescence, nuclei were stained with Hoechst (in *blue*) and cell membranes associate proteins by using with anti-β1 integrin antibody (*red*). *Scale bar:* 25 μm.

Supplementary Table 1. Patient-Derived Gastric Tissue and Cultures and Their Use in This Study

Figure	Panel	No. of samples and tissue name	No. of samples and culture name
1	*A*	1×[a] GAT26	—
1	*B*	1× GAT26A	—
1	*C*	1× GAT26C	—
1	*D*	1× GAT26A, 1× GAT26C	—
1	*E*	—	1× GAT16 A&C, 1× GAT24 A&C
1	*F, G, H*	—	1× GAT23A&C, 1× GAT24A&C, 1× GAT26A&C
2	*A*	1× GAT26C	—
2	*B*	—	3× GAT23C, 3× GAT26C
2	*C, D*	—	2× GAT17C, 2× GAT31C
2	*E*	—	2× GAT23A, 2× GAT26C
2	*F*	1× GAT26C, 1× GAT26C, 1× GAT29C	—
2	*G*	2× GAT26C, 2× GAT28C	—
3	*A, B, C*	—	2× or 3× GAT23C, 2× GAT26C
3	*D*	—	3× or 4× GAT23C, 3× or 5× GAT26C
3	*E, F*	—	2× GAT17C, 2× GAT31C
3	*G*	2× GAT25C, 2× GAT29C	—
3	*H, I, J*	—	2× GAT23C, 2× GAT 26C
4	*A*	1× GAT26C	—
4	*B*	—	3× GAT23C, 2× GAT26C
4	*C, D*	—	2× GAT23C, 2× GAT 26C
4	*E*	—	2× GAT23C, 2× GAT26C
4	*F*	—	2× GAT23C, 2× GAT26C
4	*G, H*	—	2× GAT26C
5	*A*	—	1× GAT26C
5	*B*	—	3× GAT23C, 2× GAT26C
5	*C, E, F*	—	3× GAT23C, 2× GAT26C
5	*D*	—	5× GAT 23C 4× GAT26C
5	*G, H*	—	2× GAT26C
5	*I*	—	2× GAT28C
6	*A, J*	Details provided in Supplementary Table 3	—
7	*A–C*	N/A	—
S1		N/A	—
S2	*A*	—	1× GAT23C, 1× GAT24C, 1×GAT25C, 1× GAT26C
S2	*B, C*	—	2× GAT17C, 2× GAT31C
S3	*A–E*	2× GAT26C, 2× or 3× GAT28C	1× GAT26C
S4	*A–C*	—	1× GAT26A
S5	*A, B*	—	1× GAT17C, 1× GAT31C

Supplementary Table 1. Continued

Figure	Panel	No. of samples and tissue name	No. of samples and culture name
S5	*C*	—	1× GAT28C
S6	A	—	5× GAT23C, 4× or 5× GAT26C

Code	Date of isolation	Age, *y*	Sex	Comments
GAT16	07-14-2015	34	Male	BMI: 56 kg/m^2, *Helicobacter pylori*–negative
GAT17	07-14-2015	30	Female	BMI: 53 kg/m^2, *H pylori,* not tested
GAT23	04-15-2016	55	Female	BMI: 45 kg/m^2, *H–pylori* –negative
GAT24	09-30-2016	47	Male	BMI: 36 kg/m^2, *H pylori*–negative
GAT25	01-17-2017	50	Female	BMI: not available
GAT26	02-17-2017	69	Female	BMI: 50 kg/m^2, *H–pylori*–negative
GAT27	05-10-2017	36	Female	BMI: 69 kg/m^2, *H–pylori*–negative, type 2 diabetes
GAT28	05-16-2017	32	Male	BMI: 43 kg/m^2, *H–pylori*–negative
GAT29	05-16-2017	43	Female	BMI: 48 kg/m^2, *H–pylori*–negative
GAT30	04-12-2017	53	Female	BMI: 58 kg/m^2, *H–pylori*–negative
GAT31	03-22-2019	42	Male	BMI: 60 kg/m^2, *H–pylori,* not tested

A, antrum; BMI, body mass index; C, corpus; GAT, gastric adipose tissue; N/A, Not Applicable.
[a]Numbers (eg, 1×, 2×) indicate the number of times that the specific tissue or mucosoid was used in an experiment.

Supplementary Table 2. Composition of the Culture Medium

Name	Concentration	Manufacturer	Code
Advanced DMEM/F12	18.45% v/v	Thermo Fisher	12634
Conditioned Wnt3A-medium	50% v/v	—	—
Conditioned R-spondin1 medium	25% v/v	—	—
HEPES	10 mM	Thermo Fisher	15630-056
Glutamax	1% v/v	Thermo Fisher	35050-087
B27	2% v/v	Thermo Fisher	17504044
N2	1% v/v	Thermo Fisher	17502048
Human EGF	20 ng/mL	Thermo Fisher	PHG0311
Human NOGGIN (Peprotech)	150 ng/mL	Peprotech	120-10C-1000
Human fibroblast growth factor 10	150 ng/mL	Peprotech	100-26-1000
Nicotinamide	10 mM	Sigma	N0636
Human gastrin	10 nM	Sigma	G9145
A83–01	1 μM	Calbiochem	616454
Y-27632[a]	7.5 μM	Sigma	Y0503

DMEM, Dulbecco's modified Eagle medium.
[a]After the third day the concentration is reduced to 1.5 μM.

Supplementary Table 3. Patients Biopsies From Corpus

					Antrum				Incisura				Corpus					
ID	Sex	Age, *y*	Group	*H pylori* status[a]	Activity	Chronicity	Atrophy	IM	Activity	Chronicity	Atrophy	IM	Activity	Chronicity	Atrophy	IM	OLGA	OLGIM
208	F	51	AG	2	2	2	0	2	1	2	1	0	2	2	1	0	I	II
46	F	50	AG	2	1	2	1	0	1	3	2	1	1	2	1	0	II	I
47	F	84	AG	2	0	2	1	1	0	1	0	2	1	2	1	1	II	II
90	M	54	AG	0	0	1	0	0	1	2	0	0	1	2	2	0	II	0
104	F	41	AG	0	0	1	0	0	0	1	0	0	1	2	3	2	II	II
106	F	79	AG	0	0	1	0	1	0	1	0	0	1	2	3	0	II	I
50	M	67	AG	2	2	3	2	1	2	3	2	1	2	3	2	1	III	I
69	F	71	AG	0	0	1	1	2	0	1	2	2	0	2	2	2	III	III
78	F	72	AG	0	0	2	1	0	0	2	1	0	0	3	3	1	III	I
337	M	61	AG	2	2	2	3	2	2	2	3	0	2	2	1	0	III	II
216	M	65	AG	2	2	2	3	2	2	2	3	2	2	2	3	0	IV	II
27	F	60	CG	2	0	2	0	0	0	3	0	0	0	2	0	0	0	0
58	F	74	CG	1	0	2	0	0	0	2	0	0	1	2	0	0	0	0
61	F	51	CG	2	1	2	x	0	1	2	x	0	1	2	0	0	0	II
98	F	19	CG	2	1	2	0	0	1	2	0	0	1	1	0	0	0	0
99	M	42	CG	2	1	2	0	0	1	2	0	0	2	2	0	0	0	0
111	F	46	CG	2	1	2	0	0	1	2	0	0	2	2	0	0	0	0
115	F	50	CG	1	0	1	0	0	1	2	0	0	1	2	0	0	0	0
121	F	51	CG	2	1	2	0	0	2	2	0	1	2	2	0	0	0	I
122	F	56	CG	2	1	2	0	0	1	1	0	0	1	1	0	0	0	0
160	M	74	CG	1	1	2	0	0	1	2	0	0	1	2	0	0	0	0
351	M	26	CG	0	1	2	0	0	1	1	0	0	1	1	0	0	0	0
33	M	20	N	0	0	0	0	0	0	0	0	0	0	0	0	0	0	0
40	F	65	N	0	0	1	0	0	0	1	0	0	0	1	0	0	0	0
48	F	88	N	0	0	0	0	0	0	0	0	0	0	0	0	0	0	0

Supplementary Table 3. Continued

					Antrum				Incisura				Corpus					
ID	Sex	Age, *y*	Group	*H pylori* status[a]	Activity	Chronicity	Atrophy	IM	Activity	Chronicity	Atrophy	IM	Activity	Chronicity	Atrophy	IM	OLGA	OLGIM
55	M	61	N	0	0	0	0	0	0	1	0	0	0	0	0	0	0	0
56	F	31	N	0	0	1	0	0	0	0	0	0	0	0	0	0	0	0
68	M	52	N	0	0	0	0	0	0	0	0	0	0	0	0	0	0	0

NOTE. See main text for scoring of the other parameters, as well as Operative Link on Gastritis Assessment (OLGA) and Operative Link on Gastric Intestinal Metaplasia Assessment (OLGIM) staging.
CG, chronic gastritis without atrophy; F, female; IM, intestinal metaplasia; M, male; N, normal without inflammation.
[a]0 = negative, 1 = serology positive, 2 = serology and direct proof by histology, microbiology, or rapid urease test.

Supplementary Table 4. Histology

Antibody	Host	Dilution	Manufacturer	Code
HK-ATPase-β	Mouse	1:100	Abcam	2G11
E-Cadherin	Mouse	1:100	BD Bioscience	610181
Ki67	Mouse	1:100	Cell Signaling	805
Ki67	Rabbit	1:100	Cell Signaling	D2H10
MUC6	Rabbit	1:100	Abcam	ab49462 and ab223846
MUC5AC	Mouse	1:100	Abcam	ab3649
Noggin	Mouse	1:100	Santa Cruz	2C10; sc-293439
Pepsinogen II	Sheep	1:100	Abcam	ab9013
Pepsinogen C	Rabbit	1:100	Sigma	HPA031718
β-catenin	Rabbit	1:100	Sigma-Aldrich	C2206
MIST1/bHLHa15	Rabbit	1:50	Cell Signaling	14896T
Integrin β1	Mouse	1:50	Abcam	ab30394
HK-ATPase-α	Rabbit	1:200	Abcam	ab122537
Ezrin	Rabbit	1:200	Cell Signaling	3145
EGF	Rabbit	1:50	NovisBio	NBP1-19806

Supplementary Table 5. Primers

Gene name	Primers
GAPDH	Sequence (5′ → 3′)
Forward primer	GGTATCGTGGAAGGACTCATGAC
Reverse primer	ATGCCAGTGAGCTTCCCGTTCAG
C1orf43	Sequence (5′ → 3′)
Forward primer	GGTGAATGTCGTGCTGGTG
Reverse primer	GGGATCTCAGAGGTACGAATGG
PGC	Sequence (5′ → 3′)
Forward primer	TGTCTTTGGGGGTGTGGATAG
Reverse primer	ATGAGGAACTCTTCAATGCCAATC
MUC6	Sequence (5′ → 3′)
Forward primer	CAGCTCAACAAGGTGTGTGC
Reverse primer	TGGGGAAAGGTCTCCTCGTA
MUC5AC	Sequence (5′ → 3′)
Forward primer	GGAGGTGCCCACTTCTCAAC
Reverse primer	CTTCAGGCAGGTCTCGCTG
ATP4B	Sequence (5′ → 3′)
Forward primer	TGGGTGTGGATCAGCCTGTA
Reverse primer	CTGGTCTTGGTAGTCCGGTG
ID1	Sequence (5′ → 3′)
Forward primer	GTGCTGCTCTACGACATGAAC
Reverse primer	CTTCAGCGACACAAGATGCG
LGR5	Sequence (5′ → 3′)
Forward primer	CTCCCAGGTCTGGTGTGTTG
Reverse primer	GCTCGCAATGACAGTGTGTG
BMP4	Sequence (5′ → 3′)
Forward primer	TAGCAAGAGTGCCGTCATTCC
Reverse primer	GCGCTCAGGATACTCAAGACC
EGF	Sequence (5′ → 3′)
Forward primer	GACCGGAAGTACTGTGAAGATGTT
Reverse primer	ATTGCGTGGACAGGAAACAAG
AREG	Sequence (5′ → 3′)
Forward primer	ATTTCGGTGAACGGTGTGGG
Reverse primer	CGTATTGTCTTCTAAGCTGGACTG
HBEGF	Sequence (5′ → 3′)
Forward primer	CACTGTATCCACGGACCAGC
Reverse primer	GGCTTGGAGGATAAAGTGACTCTC
MIST1	Sequence (5′ → 3′)
Forward primer	CGGATGCACAAGCTAAATAACG
Reverse primer	GCCGTCAGCGATTTGAGTAG

Supplementary Table 6. RNA Scope Probes

Target	Reactivity	Cat no.	Supplier
BMP2	Human	430641	ACD Bio-Techne
BMP4	Human	454301	ACD Bio-Techne
EGF	Human	606771	ACD Bio-Techne
TGFA	Human	313131	ACD Bio-Techne
POLR2A	Human	310459	ACD Bio-Techne
DapB	Bacteria	312038	ACD Bio-Techne